# Kinetic Ising model in an oscillating field: Avrami theory for the hysteretic response and finite-size scaling for the dynamic phase transition

S. W. Sides,[1,2,3,*] P. A. Rikvold,[1,2,3,†] and M. A. Novotny[2,‡]
[1]*Center for Materials Research and Technology and Department of Physics, Florida State University, Tallahassee, Florida 32306-4350*
[2]*Supercomputer Computations Research Institute, Florida State University, Tallahassee, Florida 32306-4130*
[3]*Colorado Center for Chaos and Complexity, University of Colorado, Boulder, Colorado 80309-0216*
(Received 8 September 1998)

Hysteresis is studied for a two-dimensional, spin-$\frac{1}{2}$, nearest-neighbor, kinetic Ising ferromagnet in a sinusoidally oscillating field, using Monte Carlo simulations and analytical theory. Attention is focused on large systems and moderately strong field amplitudes at a temperature below $T_c$. In this parameter regime, the magnetization switches through random nucleation and subsequent growth of *many* droplets of spins aligned with the applied field. Using a time-dependent extension of the Kolmogorov-Johnson-Mehl-Avrami theory of metastable decay, we analyze the statistical properties of the hysteresis-loop area and the correlation between the magnetization and the field. This analysis enables us to accurately predict the results of extensive Monte Carlo simulations. The average loop area exhibits an extremely slow approach to an asymptotic, logarithmic dependence on the product of the amplitude and the field frequency. This may explain the inconsistent exponent estimates reported in previous attempts to fit experimental and numerical data for the low-frequency behavior of this quantity to a power law. At higher frequencies we observe a dynamic phase transition. Applying standard finite-size scaling techniques from the theory of second-order equilibrium phase transitions to this *nonequilibrium* transition, we obtain estimates for the transition frequency and the critical exponents ($\beta/\nu \approx 0.11$, $\gamma/\nu \approx 1.84$, and $\nu \approx 1.1$). In addition to their significance for the interpretation of recent experiments on switching in ferromagnetic and ferroelectric nanoparticles and thin films, our results provide evidence for the relevance of universality and finite-size scaling to dynamic phase transitions in spatially extended nonstationary systems. [S1063-651X(99)08303-8]

PACS number(s): 05.40.−a, 75.60.−d, 77.80.Dj, 64.60.Qb

## I. INTRODUCTION

The term hysteresis comes from the Greek *husterein* ($\acute{\upsilon}\sigma\tau\epsilon\rho\acute{\epsilon}\omega$) which means ''to be behind'' [1]. It describes the lagging of an effect behind its cause, as when the magnetization of a body lags behind periodic changes in the applied field. While the magnetization response of a ferromagnet in an oscillating field is probably the example most familiar to physicists and engineers [2–7], hysteresis is a quite common phenomenon. For instance, it is also seen in ferroelectrics [8–15], in which the polarization lags behind a time-varying electric field. Other examples of hysteresis include electrochemical adsorbate layers that are driven through a phase transition by an oscillating electrode potential in a cyclic voltammetry experiment [16,17], and liquid-crystalline systems driven through a phase transition by pressure oscillations [18]. Recently, a new class of superconducting materials including $DyNi_2B_2C$ [19] has shown hysteresis in the resistivity when subjected to an oscillating magnetic field. Acoustic hysteresis in crystals [20] occurs when the ultrasonic absorption coefficient changes due to oscillations in the amplitude of an ultrasonic wave.

In recent years new experimental techniques, such as magnetic force microscopy (MFM) [21–25], have been developed that permit measurements of the magnetization state and switching behavior of particles as small as a few nanometers. Ferromagnetic particles in this size range consist of a single domain in equilibrium. Together with ultrathin films, they are of interest as potential materials for ultrahigh density recording media. The dynamics of magnetization reversal in nanoscale systems has been modeled by kinetic Ising systems subject to sudden field reversal [26–31]. These numerical and analytical studies give results in qualitative agreement with the experiments mentioned above. Recent experiments on ultrathin ferromagnetic Fe/Au (001) films [32] and thin $p(1\times1)$ Fe films on W(110) [33] have considered the frequency dependence of hysteresis loop areas, which were interpreted in terms of effective exponents consistent with those found for a continuous spin model [12,34–36]. Similar experiments have been performed on ultrathin Co films on Cu(001). A study of this system by Jiang, Yang, and Wang [37] reported exponents consistent with a mean-field treatment of the Ising model, whereas a recent study by Suen *et al.* [38] found very small effective exponents in the low-frequency regime, apparently consistent with the theoretical results we report here.

The above discussion is far from an exhaustive account of hysteresis examples, but it does give an idea of the diversity of situations in which this nonlinear, nonequilibrium phe-

*Present address: Integrated Materials Research Laboratory, Sandia National Laboratory, Albuquerque, NM 87185. Electronic address: swsides@sandia.gov
†Permanent address: Florida State University, Tallahassee, FL 32306-4350. URL: http://www.scri.fsu.edu/~rikvold/. Electronic address: rikvold@scri.fsu.edu
‡URL: http://www.scri.fsu.edu/~novotny/. Electronic address: novotny@scri.fsu.edu

 

nomenon is important. Systems that exhibit hysteresis have in common a nonlinear, irreversible response which lags behind the applied force. Numerous general mathematical theories have been formulated to model hysteretic behavior in a variety of systems, including the Preisach model [6,39–41] and systems of differential equations that display discontinuous bifurcations [39,40,42]. Hysteresis in thermodynamic systems is often due to the presence of a first-order phase transition, which is the source of strong nonlinearity in the system. These details of the nonlinear response can, however, be quite different in different systems and even in different parameter regimes for the same system. The details must be carefully considered in order to accurately predict such aspects of the hysteretic response as its dependence on the frequency, amplitude, and wave form of the oscillating force. Here we present a study of hysteresis in a particular model system which incorporates both spatial degrees of freedom and thermal fluctuations, and which has a first-order equilibrium phase transition. The system response in the parameter regime studied in this paper is *self-averaging* and may be described by the Kolmogorov-Johnson-Mehl-Avrami (KJMA) theory of metastable decay [43–45].

Specifically, we consider hysteresis in a spin-$\frac{1}{2}$, nearest-neighbor, kinetic Ising ferromagnet on a two-dimensional square lattice with periodic boundary conditions, which is subject to a sinusoidally oscillating field. For convenience, and because many of the experimental measurements of hysteresis involve magnetic systems, we use the customary magnetic language in which the order parameter is the dimensionless magnetization per site, $m(t) \in [-1,+1]$, and the force is the magnetic field $H(t)$. However, we expect our results also to apply to hysteresis in other areas of science. For example, in dielectrics $m(t)$ and $H(t)$ can be reinterpreted as polarization and electric field, in adsorption problems as coverage $\theta(t)=[m(t)+1]/2$ [46] and (electro)chemical potential or (osmotic) pressure, etc.

Below its critical temperature and in zero field, this model has two degenerate ordered phases corresponding to a majority of the spins in the positive or negative direction. A weak applied field breaks the degeneracy, and the phase with the spins aligned (antialigned) with the field is stable (metastable). If the field varies periodically in time, the system is driven back and forth across a first-order phase transition at $H=0$, and the two phases alternate between being momentarily stable and metastable. As a result, $m(t)$ lags behind $H(t)$, and hysteresis occurs. In the regime of large system size, moderately strong field, and temperature well below $T_c$ considered here, the system switches smoothly and almost deterministically between the two magnetized phases.

The metastable phase in Ising models subject to a sudden field reversal from $H$ to $-H$ decays by different mechanisms, depending on the magnitude of $H$, the system size $L$, and the temperature $T$. Two distinct regimes are separated by a crossover field called the dynamic spinodal, $H_{\mathrm{DSP}} \sim (\ln L)^{-1/(d-1)}$, where $d$ is the spatial dimensionality [47,48]. Detailed discussions of these different decay modes are found in Refs. [31,48,49]. At sufficiently low $T$ that the single-phase correlation lengths are microscopic, the different decay regimes can be distinguished by the interplay among four length scales: the lattice spacing $a$, the system size $L$, the radius of a critical droplet $R_c \propto 1/|H|$, and the average distance a supercritical droplet interface propagates before encountering another droplet $R_0 \propto \exp\{\Xi_0(T)/[(d+1)|H|^{d-1}]\}$. The physical significance of $\Xi_0(T)$ is explained in Sec. II. In this paper, we specifically consider decay in the multidroplet (MD) regime $[H_{\mathrm{DSP}}(T,L)<|H|<H_{\mathrm{MFSP}}(T)$ where $R_c(H_{\mathrm{MFSP}}) \approx 0.5]$. In terms of the characteristic lengths, the MD regime is defined by

$$a \ll R_c \ll R_0 \ll L. \tag{1.1}$$

Here the decay of the metastable phase proceeds by random homogeneous nucleation of *many* critical droplets of the stable phase, which then grow and coalesce. The MD regime is distinct from the strong-field regime, $|H| > H_{\mathrm{MFSP}}(T)$. It is also distinct from the single-droplet (SD) regime $[|H|<H_{\mathrm{DSP}}(T,L)]$, where $a \ll R_c \ll L \ll R_0$. In the SD regime, the decay of the metastable phase proceeds by random homogeneous nucleation of a *single* critical droplet of the stable phase. Hysteresis in that regime is described in detail in Ref. [50]. The present study, as well as our previous work [51,52], shows that the response to an oscillating field is significantly different in the MD and SD regimes.

Theoretical and computational studies of hysteresis have been performed for several models, using a variety of methods [53]. These include various studies of models with a single degree of freedom, equivalent to mean-field treatments of the Ising model [54–56], Monte Carlo (MC) simulations of the spin-$\frac{1}{2}$ Ising model [35,36,57–66], and several O($N$) type models [12,34–36,67]. These studies were performed with variations in the details of the simulations and in the model parameters. Most of them indicate that the average hysteresis-loop area appears to display power-law dependences on the frequency and amplitude of $H(t)$. However, there is no universal agreement on the values of the exponents, either experimentally or theoretically. For the Ising model it has been pointed out that nucleation effects would lead to an asymptotically logarithmic frequency dependence [11,29,35,68]. A mean-field model exhibits a dynamic phase transition in which the mean period-averaged magnetization changes from a nonzero value to zero [55]. Such a dynamic phase transition has been observed in MC simulations of a kinetic Ising model as well [57–62,64–66,69]. A fundamentally different example of criticality in a hysteretic system is the zero-temperature, random-field Ising model, which exhibits critical behavior in the hysteresis loop as a function of disorder [70].

The work presented in this paper and in Refs. [50–52,69] differs from most past theoretical and numerical studies of hysteresis in two important ways. First, mean-field models do not take into account thermal noise and spatial variations in the order parameter, thus ignoring fluctuations which may be important in real materials. Second, most previous investigations of hysteresis in Ising models have considered the frequency and amplitude dependence of quantities such as the loop area and the period-averaged magnetization *without* considering the manner in which the metastable phase decays. In this paper, the long-time behavior of the hysteretic response is analyzed by studying the power spectral densities of the magnetization time series as well as the statistical properties of the period-averaged magnetization $Q$, the loop area $A$, and the correlation $B$. These quantities are defined as

$$Q=\frac{\omega}{2\pi}\oint m(t)dt, \tag{1.2}$$

$$A=-\oint m(H)dH, \tag{1.3}$$

$$B=\frac{\omega}{2\pi}\oint m(t)H(t)dt, \tag{1.4}$$

where the initial time $t_0$ of the period is defined such that $H(t_0)=H(t_0+2\pi/\omega)=0$.

Due to the multidroplet decay mechanism, the average hysteresis-loop area exhibits an extremely slow crossover to a logarithmic decay with frequency and amplitude in the asymptotic low-frequency limit [52]. This asymptotic behavior of the loop area in the MD regime is qualitatively similar to that for the SD regime for two dimensions [50,52]. However, the calculation is somewhat more involved, and the quantitative behavior of the loop area is different for the two regimes.

Beside our results on the low-frequency loop areas, our most significant finding is detailed evidence of finite-size scaling at a dynamic phase transition (DPT) in the MD regime. Here we provide a full account of these results, which we briefly reported in Ref. [69]. This transition can be intuitively understood as a competition between two time scales: the period of the external field, $2\pi/\omega$, and the average lifetime of the metastable phase, $\langle\tau(H)\rangle$, defined as the first-passage time to a magnetization of zero following an instantaneous field reversal from $H$ to $-H$. If $2\pi/\omega\ll\langle\tau(H_0)\rangle$ [$H_0$ is the amplitude of $H(t)$] the magnetization cannot fully switch sign within a single period, and $|Q|>0$. We shall refer to this situation as the ordered dynamic phase. If $2\pi/\omega\gg\langle\tau(H_0)\rangle$ the magnetization follows the field, and $Q\approx 0$. This is the disordered dynamic phase. Between these limits there is a critical frequency at which $\langle|Q|\rangle$ appears to become singular in the infinite-system limit. We emphasize that the DPT is a nonequilibrium phase transition, and that the probability distribution of the system magnetization which characterizes the two phases never relaxes into a stationary state. However, the ''filtered'' time series of $Q$ for successive field periods is a stationary stochastic process. To avoid confusion we establish the following terminology. By the term ''dynamic phase'' we mean one of the qualitatively different system responses separated by the DPT. In contrast, the term ''phase'' by itself refers in the conventional way to a uniform thermodynamic phase.

The rest of this paper is organized as follows. Details of the model and a brief review of relevant aspects of the Avrami theory of metastable decay are given in Sec II. Time-series data for the magnetization and the period-averaged magnetization $Q$ are discussed in Sec. III. In Sec. IV we discuss the power spectral densities obtained from the time-series data. In Sec. V we obtain an analytical result for the time-dependent system magnetization during a single period of the field, based on the droplet theory of nucleation and a time-dependent extension of the Avrami theory. Section VI contains an analysis of the hysteresis-loop area $A$ and the correlation $B$. This section includes MC data for the probability distributions and averages of $A$ and $B$ along with theoretical predictions based on the results in Sec. V. In Sec. VII we consider the period-averaged magnetization $Q$, which is the order parameter for the dynamic phase transition. Details of the finite-size scaling analysis for this transition are given in this section as well. A summary, discussion, and topics for future study are presented in Sec. VIII.

## II. MODEL

The model used in this study is a kinetic, nearest-neighbor Ising ferromagnet on a hypercubic lattice with periodic boundary conditions. The Hamiltonian is given by

$$\mathcal{H}=-J\sum_{\langle ij\rangle}s_is_j-H(t)\sum_i s_i, \tag{2.1}$$

where $H(t)=-H_0\sin(\omega t)$, $s_i=\pm 1$ is the state of the $i$th spin, $\Sigma_{\langle ij\rangle}$ runs over all nearest-neighbor pairs, and $\Sigma_i$ runs over all $N=L^d$ lattice sites. The magnetization per site is

$$m(t)=\frac{1}{L^d}\sum_{i=1}^{N}s_i(t). \tag{2.2}$$

The dynamic used is the Glauber [71] single-spin-flip Monte Carlo algorithm with updates at randomly chosen sites. The time unit is one Monte Carlo step per spin (MCSS). The system is put in contact with a heat bath at temperature $T$, and each attempted spin flip from $s_i$ to $-s_i$ is accepted with probability [72]

$$W(s_i\rightarrow -s_i)=\frac{\exp(-\beta\Delta E_i)}{1+\exp(-\beta\Delta E_i)}. \tag{2.3}$$

Here $\Delta E_i$ is the change in the energy of the system that would result if the spin flip were accepted, and $\beta=1/k_BT$ where $k_B$ is Boltzmann's constant. It has been shown in the weak-coupling limit that the stochastic Glauber dynamic can be derived from a quantum-mechanical Hamiltonian in contact with a thermal heat bath modeled as a collection of quasi-free Fermi fields in thermal equilibrium [73].

The average number of droplets of the stable phase that are formed per unit time and volume is given by the field- and temperature-dependent nucleation rate per unit volume,

$$I(H(t),T)\approx B(T)|H(t)|^K\exp\left[-\frac{\Xi_0(T)}{|H(t)|^{d-1}}\right]. \tag{2.4}$$

The notation follows that of Ref. [26], where $B(T)$ is a nonuniversal temperature-dependent prefactor, and $K$ and $\Xi_0(T)$ are known from field theory [74,75], MC simulations [48] and numerical transfer-matrix calculations [76,77]; their values are listed in Table I. The quantity $\Xi_0(T)$ is the field-independent part of the free-energy cost of a critical droplet, divided by $k_BT$. The field, $H(t)$, is the only quantity through which $I(H(t),T)$ depends on time in this adiabatic approximation.

Several other quantities, whose values do not depend on the frequency of the field, are required as input for the theoretical calculations in the following sections and are listed in Table I. They are determined through what we refer to as ''field-reversal simulations.'' In these simulations the system

TABLE I. Parameters and constants used in this work. The values of the parameters $H_0$, $L$, and $T$ have been selected such that switching occurs via the multidroplet mechanism. The constants $\Xi_0(T)$ and $K$ are calculated from droplet theory [74–77] for two-dimensional Ising systems. The constants $\langle\tau\rangle$ and $r$ are measured from field-reversal MC simulations with the Glauber dynamic (using the parameters listed in the left column). The constants $\Omega(T)$ [77] and $\nu(T)$ [79], where the droplet interface velocity is $v_0 = \nu(T)|H|$, have been measured in other work. The value for $H_{\rm DSP}$ is taken from Fig. 11 of Ref. [80]. For $L=90$ and 128, the relative standard deviation is $r=0.072$ and 0.053, respectively. Except for $H_{\rm DSP}$, which decreases slowly with increasing $L$, all other values are the same for $L=90$ and $L=128$.

| Parameters | | Constants (theory) | | Constants (simulation) | |
|---|---|---|---|---|---|
| $H_0$ | $0.3J$ | $\Xi_0(T)$ | $0.506192J$ | $\Omega_2(T)$ | 3.15255 |
| $L$ | 64 | $K$ | 3 (exact) | $\nu(T)$ | $(0.465\pm0.014)J^{-1}$ MCSS$^{-1}$ |
| $T$ | $0.8T_c$ | | | $\langle\tau\rangle$ | 74.5977 MCSS |
| | | | | $H_{\rm DSP}(L=64)$ | $(0.11\pm0.005)J$ |
| | | | | $r(L=64)$ | 0.105 |

initially has all spins up, i.e., positive. It is then subjected to a static field of magnitude $H_0$ with a sign opposite the system magnetization. This instantaneous field quench prepares the system in a metastable state, and the decay of this metastable phase proceeds by the MD mechanism outlined in Sec. I.

In the MD parameter regime the average size of a critical droplet $R_c$ and the average distance between droplets $R_0$ are both much smaller than the system size. Therefore, many droplets nucleate and grow to drive the system into the stable phase, resulting in an almost deterministic decay process. This can be understood by imagining the system subdivided into cells of linear size $R_0$, which each contain a single droplet. Each of these subsystems will appear to be in the SD regime, and the time taken to nucleate a critical droplet is stochastic with an exponential probability distribution. However, as a consequence of the central limit theorem the probability density of the lifetime for the entire system asymptotically approaches a Gaussian as the system size increases. The decay process thus becomes increasingly deterministic, with a lifetime distribution whose variance decreases as $L^{-d}$ with increasing system size [26].

In addition to the ''self-averaging'' process described above, two other concepts are needed to understand the MD decay process: the droplet interface velocity and the overlapping of growing supercritical droplets. Our detailed treatment of these effects is given in Sec. V, where the theory of MD decay in a static field is generalized to time-dependent fields. Accounting for all of these effects, an expression may be obtained for the time-dependent magnetization of a system in a field-reversal experiment. In the KJMA approximation [43–45], it is assumed that the positions and sizes of the growing droplets are uncorrelated. In the simple field-reversal case this leads to the well known ''Avrami's law''

$$m(t)=2\exp[-\Phi(t)]-1 \tag{2.5a}$$

$$=2\exp\left[-\int_0^t I\Omega_d(v_0t')^d dt'\right]-1 \tag{2.5b}$$

$$=2\exp\left[-\frac{\Omega_d v_0^d I}{d+1}t^{d+1}\right]-1, \tag{2.5c}$$

where $v_0$, the interface velocity for a growing droplet of the stable phase, is assumed to be constant, $\Omega_d$ is a proportionality constant such that the volume $V$ of a droplet of radius $R$ is $V=\Omega_d R^d$, and the other constants have been introduced previously. The integral $\Phi(t)$ in Eq. (2.5) is the ''extended volume'' [45], i.e., the total volume fraction of droplets of the equilibrium phase at time $t$, *uncorrected* for overlaps. The assumption that the positions and sizes of the droplets are uncorrelated leads directly to the exponential relation for $m(t)$ [78]. Solving Eq. (2.5c) for the time at which $m=0$ gives the average lifetime in the MD regime,

$$\langle\tau\rangle=\left[\frac{\Omega_d v_0^d I}{\ln 2(d+1)}\right]^{-1/(d+1)}, \tag{2.6}$$

which, in contrast to the SD regime, is independent of $L$. To describe the hysteretic response in the MD regime, in Secs. V and VI we employ a time-dependent extension of this theory, in which $I$ and $v_0$ are both functions of time through $H(t)$.

## III. TIME-SERIES DATA

All numerical simulations reported in this paper are performed for $d=2$, $T=0.8T_c$ and one of three system sizes $L=64$, 90, and 128. A sinusoidal field is applied to the system with amplitude $H_0=0.3J>H_{\rm DSP}(L)$, chosen such that in field-reversal simulations the system is clearly in the MD regime for a field of magnitude $H_0$ for all three values of $L$.

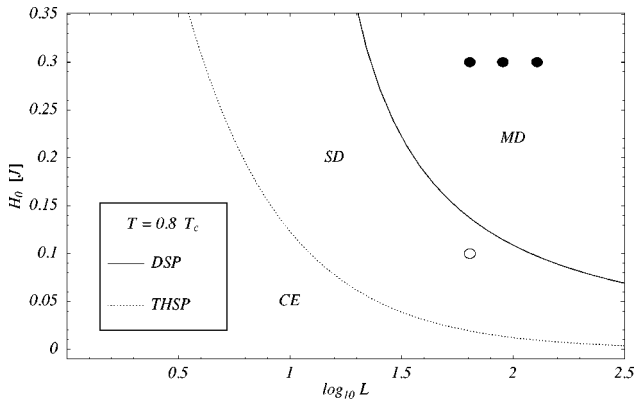


FIG. 1. Location of MD simulations in the $(H_0, L)$ plane. The solid curve represents the dynamic spinodal (DSP) $H_{\mathrm{DSP}} \sim (\ln L)^{-1/(d-1)}$. This theoretical curve is an asymptotic result obtained by setting $R_0 \approx L$. The filled circles denote the system sizes ($L=64$, 90, and 128) and field amplitude ($H_0=0.3J$) used here to study hysteresis in the MD regime. The open circle denotes the system size and field amplitude used to study hysteresis in the SD regime in Ref. [50]. The dotted curve represents a theoretical result for the ''thermodynamic spinodal field'' (THSP) [47,48] which separates the SD region from the coexistence regime (CE). It is obtained by setting $R_c \approx L$.

This is illustrated in Fig. 1. The dynamic spinodal field is approximated by $H_{\mathrm{DSP}} \approx H_{1/2}$, where $H_{1/2}$ is the value of $H$ (for given $L$ and $T$) for which the relative standard deviation of the lifetime, $r = \sigma_\tau / \langle \tau \rangle$ is 1/2 ($\sigma_\tau$ is the standard deviation of the lifetime). The values of $H_{\mathrm{DSP}}$ and $\langle \tau \rangle$ for $T = 0.8 T_c$ and $L=64$ [79,80] are given in Table I. For the larger systems, $\langle \tau \rangle$ is approximately unchanged, while $H_{\mathrm{DSP}}$ and $r$ are smaller than for $L=64$. At this temperature, $H_{\mathrm{MESP}} \approx 0.75J > H_0$. Thus the system is well within the MD regime for all three sizes used.

To obtain the raw time-series data, the system was initially prepared with either a random arrangement of up and down spins with $m(t=0) \approx 0$, or with a uniform arrangement with all spins up. Then the sinusoidal field was applied and changed every attempted spin flip, allowing for a smooth variation of the field. The time series did not appear to depend on the initial conditions after a few periods. For each system size, the simulations were performed with several values of the driving frequency $\omega$. For each frequency, we recorded the time-dependent magnetization $m(t)$. Most of the simulations at intermediate and high frequencies were recorded for approximately $16.9 \times 10^6$ MCSS. (Simulations for some of the lowest frequencies were recorded for approximately $5.9 \times 10^5$ MCSS.) Files containing the data for these longest runs are about 800 megabytes and required nine days (one month) to run for $L=64$ ($L=128$) on a single 66 MHz node of an IBM sp2 computer. Since the hysteresis depends on the competition between the two time scales represented by the field period and the metastable lifetime, we chose the frequencies of $H(t)$ by specifying the ratio

$$R = \frac{(2\pi/\omega)}{\langle \tau(H_0) \rangle}. \tag{3.1}$$

One may think of $R$ as a scaled period, and $1/R$ as a scaled frequency.

We note that $\langle \tau(H_0) \rangle$ is the ''shortest of the long time scales'' that describe the system. For $T = 0.8 T_c$ and all the values of $L$ used here, the time scale for spontaneous fluctuations between the phases in the absence of an applied field, $\langle \tau(0) \rangle$, is essentially infinite. Even when the field has its maximum strength $H_0$, the nucleation of the critical droplets necessary to leave the metastable phase is always driven by the thermal fluctuations. Driving the system from the metastable to the stable phase therefore truly depends on the joint action of the random thermal noise and the deterministic oscillating field. Figure 2 shows short initial segments of the magnetization time series for four different values of $R$. The figures for the first three values of $R$ are chosen to represent: a system in the ordered dynamic phase ($R=3$, $\langle |Q| \rangle > 0$), near the dynamic transition ($R = 3.436 \approx R_{\mathrm{cr}}$), and in the disordered dynamic phase ($R=7$, $\langle |Q| \rangle \approx 0$). This value for $R_{\mathrm{cr}}$ is obtained by finite-size scaling analysis of the probability density for $Q$, as described in Sec. VII. The time-series segment shown for $R=200$ is deep in the disordered dynamic phase region and illustrates the behavior of the system for very low frequencies. The standard deviation of the average lifetime in the MD regime is relatively small compared to the SD regime. If the period of $H(t)$ is sufficiently long, the system has enough time to switch phases during a single half-period. This is clearly seen at $R=7$, for which the system switches during practically every half-period. Soon after $m(t)$ reaches saturation, the field passes through zero and favors the opposite phase. Similar behavior is seen in the time series for $R=200$, except that the period is so long that the system decays to the favored phase well before the field reaches its maximum value. Then the magnetization fluctuates near its equilibrium value $m(t) \approx \pm 1$ until the field again switches sign and the system once more becomes metastable. If the period of $H(t)$ is sufficiently short, the system does not have time to switch during a single half-period. This can be seen for $R=3$. While the field favors the opposite phase, the magnetization changes as many critical droplets nucleate and begin to grow. Before the magnetization can completely reverse, however, the field changes sign and the droplets of the now unfavored phase shrink and disappear. For $R=3.436$, the period near the critical value, the period-averaged magnetization slowly ''meanders'' from positive to negative values over several periods of $H(t)$. This ''slow switching'' occurs many times over the entire time series. The number of field cycles shown in Fig. 2 is small compared to the total number of cycles in an entire time series.

The ''slow switching'' seen near the dynamic phase transition also occurs for frequencies in the ordered dynamic phase region, where $\langle |Q| \rangle > 0$. However, there the times between consecutive switches are too long to show in plots of $m(t)$ vs $t$. For this reason, the ''filtered time series'' for $Q$ are shown in Fig. 3, which provide plots of $Q$ for consecutive periods in the magnetization time series. Even for the $Q$ time series, the number of periods shown is small compared to the total number of periods, except for $R=200$ which displays the entire time series. For the low frequencies, the $Q$ values are concentrated near $Q=0$, with larger fluctuations for $R=7$ than for $R=200$. Analysis of the $Q$ data and the dynamic phase transition will be detailed in Sec. VII.

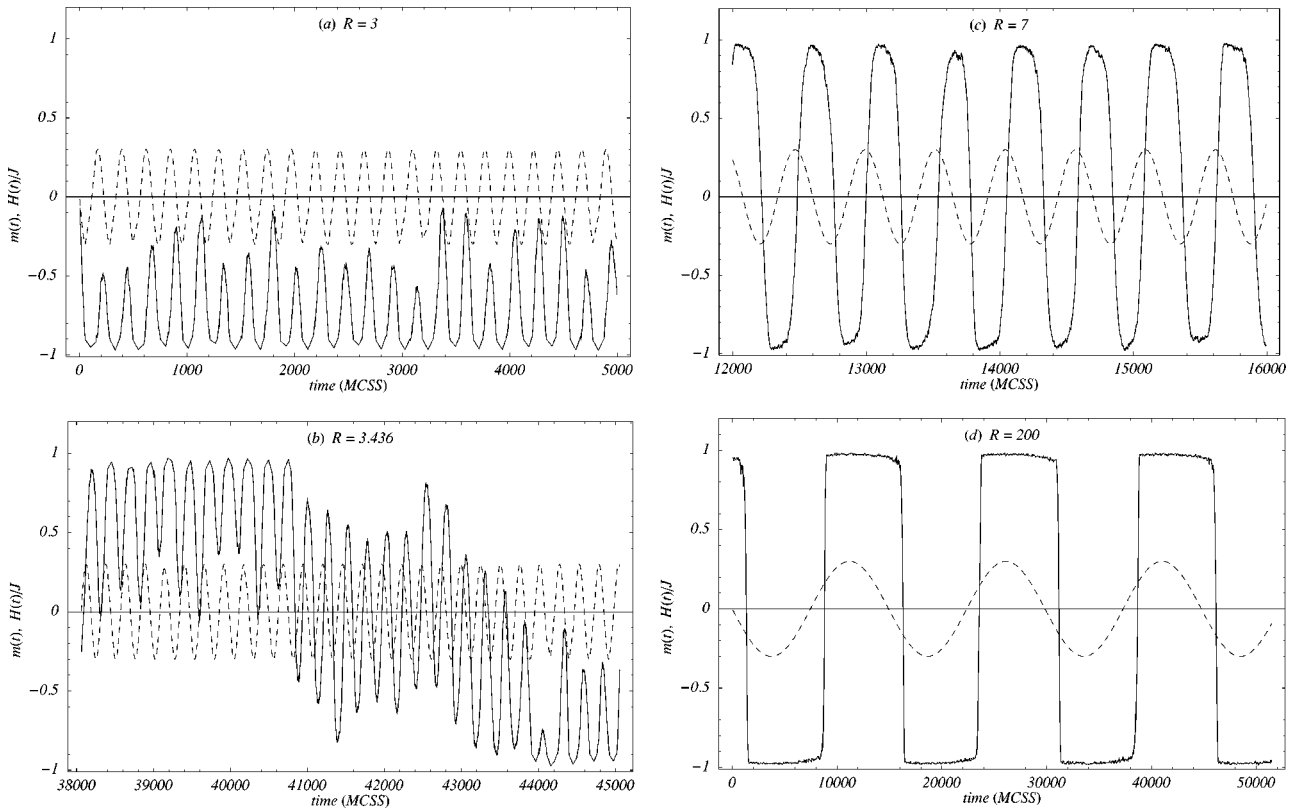


FIG. 2. Short segments of the magnetization time series $m(t)$ (solid curve) and the external field $H(t)$ (dashed curve) vs time $t$ for $T=0.8T_c$, $d=2$, $L=64$, and $H_0=0.3J$. The total lengths of the time series are approximately $16.9\times10^6$ MCSS. For these parameter values the average lifetime in a static field is $\langle\tau(H_0)\rangle\approx75$ MCSS. The time series are shown for the scaled field periods (a) $R=3$, (b) $R=3.436\approx R_{\rm cr}$, (c) $R=7$, and (d) $R=200$.

## IV. POWER SPECTRAL DENSITIES

A standard method used to characterize a time series is to calculate its power spectral density (PSD). Figure 4 shows the PSD's of the raw data, short segments of which are shown in Fig. 2. The technical details on how the PSD's were obtained are elaborated upon in Ref. [50]. For clarity, the PSD's for different driving frequencies, shown in Fig. 4(a) with $L=64$, have been shifted in the vertical direction by arbitrary offsets. The same spectra are plotted in Fig. 4(b) with no offset. The fourth spectrum shown in Fig. 4, labeled ''background,'' corresponds to thermal equilibrium fluctuations in a single thermodynamic phase. To obtain this spectrum, a simulation was performed on a system with the same size, temperature, and for the same number of MCSS as the other spectra, in a *static* field of $H_0/\sqrt{2}$.

To describe the PSD for each frequency, we identify three distinct regions: (1) the peaks, (2) the thermal noise region, and (3) the low-frequency region. The most prominent features of the PSD's are the sharp peaks. For $R=3$ and $R=3.436\approx R_{\rm cr}$, the first peak in the spectrum corresponds to $\omega$, the frequency of the external field; the second peak corresponds to $2\omega$; and so on. These odd and even harmonic peaks arise because the shape of the time series is not purely sinusoidal due to the nonlinear response of the system. For $R=7$ (and longer periods), only odd harmonics are seen. The extinction of the even harmonic peaks occurs because the shape of the time series is beginning to resemble a square wave (see Fig. 2). The power $p_n$ contained in the $n$th component of the Fourier series for a pure square wave is $p_n=16[\sin(n\pi/2)]^4/(n\pi)^2$, which decays as $n^{-2}$ and vanishes for even $n$. This enables one to understand the reduced second harmonic in the PSD for $R=7$, which is just barely observable between the first two sharp peaks. However, in contrast to our observations in the SD regime [50], no dips in the PSD at even $n$, corresponding to the zeros of $p_n$ [81], were observed for the values of $R$ analyzed here.

Unlike the SD regime [50], the highest frequencies for each of the PSD's do not fall onto the thermal noise background. Since the average lifetime in the MD regime is much smaller than in the SD regime, the $R$ values shown in Fig. 4 correspond to much larger frequencies in units of $\mathrm{MCSS}^{-1}$. Therefore, the time scales characterizing the peaks and the thermal noise regions are not as well separated as for the SD regime, so the two regions overlap. Also, none of the PSD's shown here are for low enough frequencies that the metastable phase can decay and the system remain in the stable state sufficiently long during each half-period to sample the purely thermal fluctuations which would display exponential time correlations.

The low-frequency region comprises the portion of each spectrum between the first peak and the lowest resolved frequency. The PSD in this region exhibits a strong dependence on the frequency of the field. Significant amounts of power in this portion of a PSD indicate the presence of slow behav-

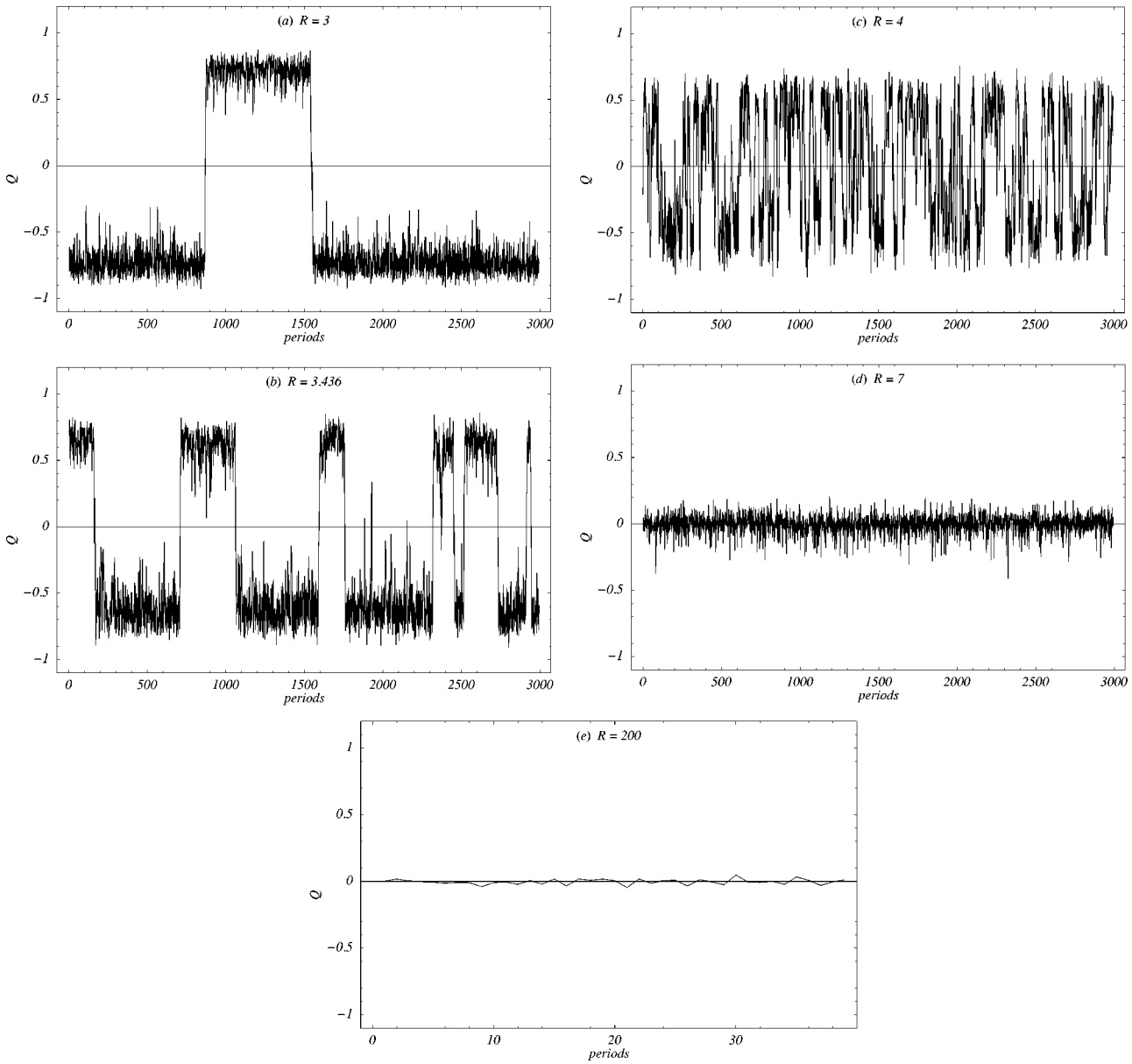


FIG. 3. Short segments of the ''filtered time series'' of period-averaged magnetization values, $Q$, vs number of field periods. The parameters used are the same as in Fig. 2. (a) $R=3$, (b) $R=3.436\approx R_{\mathrm{cr}}$, (c) $R=4$, (d) $R=7$, and (e) $R=200$.

ior on time scales larger than that of the driving field. Near the transition frequency $R=3.436\approx R_{\mathrm{cr}}$, the overall slope in the low-frequency region is close to $-2$. This suggests that the long-time correlations are exponential with a very large correlation time [82]. The turnover in the corresponding Lorentzian PSD is not observable because of the lack of low-frequency resolution due to the finite length of the time series. For $R=3$, the low-frequency region of the PSD also suggests a Lorentzian, again with a correlation time that is difficult to estimate due to the poor low-frequency resolution. For $R=7$, the flat low-frequency region is that of the PSD of white noise. This is consistent with the behavior of the $Q$ time series shown in Fig. 3(d). The PSD's for other system sizes display a qualitatively similar frequency dependence in the sharp peak and low-frequency regimes discussed above. However, there is a systematic size dependence in the PSD's for the thermal noise background, which is smaller for larger $L$. This is easily understood since the variance of the magnetization in equilibrium should be proportional to $L^{-2}$.

## V. DERIVATION OF $m(t)$ FROM AVRAMI'S LAW

The theoretical predictions for the frequency dependence of both the hysteresis-loop areas and the correlation rely on numerically solving an expression for $m(t)$ during a single field period. This expression is derived from a generalization of Avrami's law with time-dependent nucleation rate and growth velocity. Using these values for $m(t)$ in Sec. VI, we explicitly calculate the average hysteresis-loop area $\langle A\rangle=-\langle\oint m(H)dH\rangle$ and the average correlation $\langle B\rangle=(\omega/2\pi)\langle\oint m(t)H(t)dt\rangle$. Avrami's law gives the volume fraction of the metastable state for systems in which many noninteracting droplets nucleate, then grow and coa-

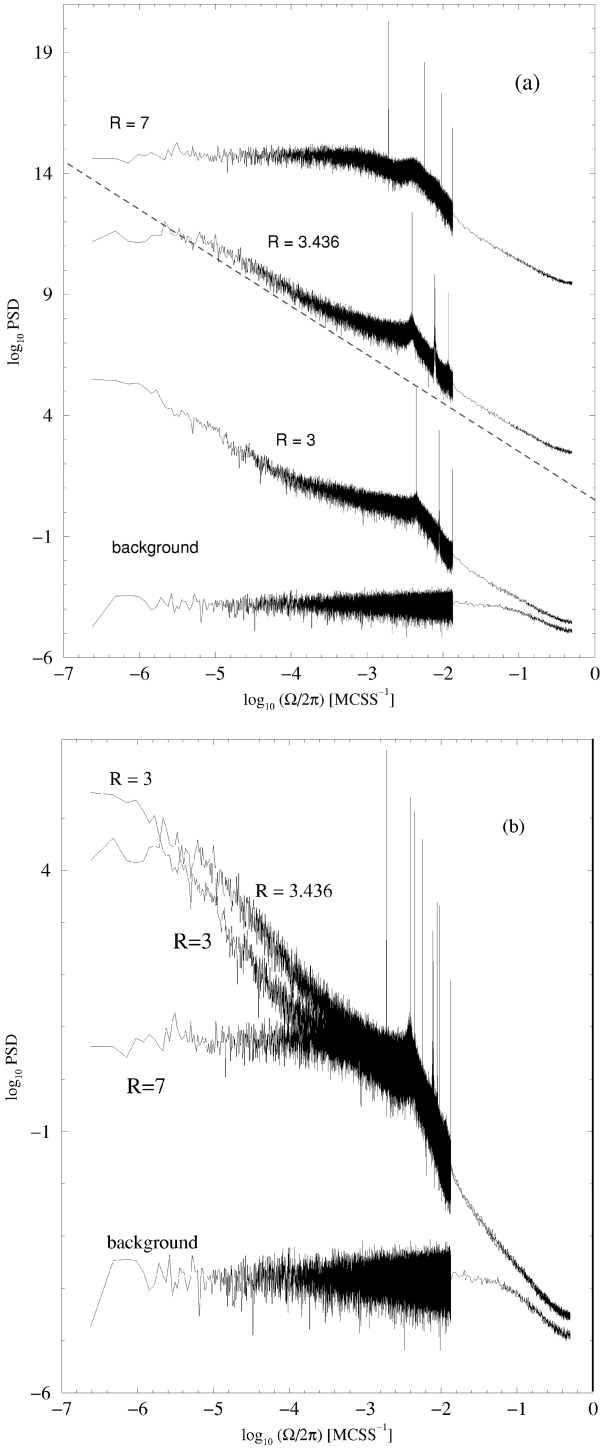


FIG. 4. (a) Power spectral densities (PSD's) for $L=64$. Spectra are shown for three different frequencies of the field, and are plotted with an arbitrary offset for clarity. In addition to a change in the amount of smoothing, the right-hand section of each spectrum contains only one out of every 250 data points to facilitate plotting. The magnetization is sampled every 1.0 MCSS, so the Nyquist frequency is $(\Omega_N/2\pi)=0.5$ MCSS$^{-1}$. The lowest frequency that can be resolved is $2.38\times10^{-7}$ MCSS$^{-1}$. The dashed line with slope $-2$ is a guide to the eye. (b) Same spectra without the offset to illustrate how all three PSD's fall near the thermal noise background at high frequencies. Note that the spectra for $R=3$ and $R=3.436\approx R_{\rm cr}$ cross at low frequencies.

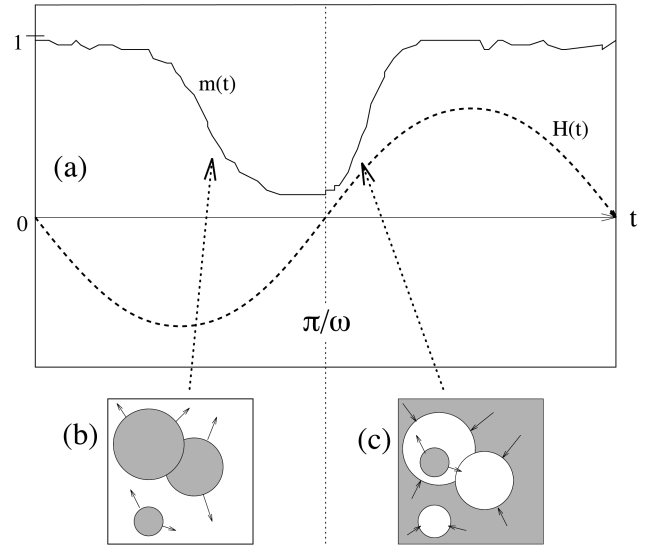


FIG. 5. Schematic of growing and shrinking droplets in the MD regime for a sufficiently high frequency such that $m(t)$ does not completely switch during a period. In (b) and (c) the dark regions represent the stable phase, and the light regions represent the metastable phase. The arrows indicate the growth direction of the droplet interfaces.

lesce without changing their shapes as the system decays to the stable phase. The volume fraction of metastable phase is related to the magnetization by $\phi(t)\approx[m(t)+1]/2$. The original KJMA calculation shows that the volume fraction of the metastable phase, $\phi(t)$, is given by Eq. (2.5a). For a homogeneous, time-dependent nucleation rate, the extended volume in Eq. (2.5b) is generalized to

$$\Phi(t)=\int_0^t I(L,T;t_{\rm n})V(t,t_{\rm n})dt_{\rm n}, \tag{5.1}$$

where $V(t,t_{\rm n})$ is the volume at time $t$ of a droplet which was nucleated at time $t_{\rm n}$, and $I(L,T;t_{\rm n})$ is the time-dependent nucleation rate given by Eq. (2.4). The volume $V(t,t_{\rm n})$ is given by

$$V(t,t_{\rm n})=\Omega_d\left[\int_{t_{\rm n}}^t v(t')dt'\right]^d. \tag{5.2}$$

The Lifshitz-Allen-Cahn approximation [83–85] is used to specify the interface velocity of a growing droplet as $v(t)\approx\nu|H(t)|$. (The proportionality factor $\nu$ should not be confused with the critical exponent $\nu$, discussed in Sec. VII.) The effects of the dependence of the proportionality factor $\nu$ on the droplet radius, which are remarkably minor, are discussed by Shneidman and co-workers [86,87]. Equation (5.1) with $d=2$ and $K=3$ in Eq. (2.4) then gives

$$\Phi(t)=\int_0^t I(L,T;t_n)\Omega_2\left[\int_{t_n}^t \nu H_0 \sin\omega t' dt'\right]^2 dt_n=\int_0^t I(L,T;t_n)\frac{\Omega_2\nu^2H_0^2}{\omega^2}[\cos\omega t_n-\cos\omega t]^2 dt_n$$

$$=\frac{B(T)\Omega_2\nu^2H_0^2}{\omega^2}\int_0^t[\cos\omega t_n-\cos\omega t]^2|H_0\sin\omega t_n|^3\exp\left[-\frac{\Xi_0(T)}{|H_0\sin\omega t_n|}\right]dt_n. \tag{5.3}$$

Numerically integrating Eq. (5.3) for $t\in[0,\pi/\omega]$ and substituting into Eq. (2.5a) enables one to find $\phi(t)=\exp[-\Phi(t)]$ for a system which starts with $\phi(0)=1$. The only quantity which must be determined from the MC simulations is $B(T)$, the field-independent part of the prefactor in the nucleation rate. In the present paper, this single parameter is set by demanding that the average simulated loop area for $R=200$ matches the theoretical prediction (see Sec. VI).

The integration of Eq. (5.3) can only be performed for the first half-period of the field cycle, in which $m(t)$ and $H(t)$ have opposite signs. When $m(t)$ and $H(t)$ have the same sign, the droplets that were formed during the previous half-period will shrink. The magnetization is therefore unable to switch sign during a single period for sufficiently high frequencies [see Fig. 5(a)]. The KJMA theory cannot be used to find the volume fraction of *shrinking* droplets of the metastable phase. Therefore, an approximate calculation of $m(t)$ for $t\in[\pi/\omega,2\pi/\omega]$ must be devised. Assume that the shrinking droplets in Fig. 5(c) are described by merely reversing the nucleation and growth process represented in Fig. 5(b). Then, the volume fraction of the growing, now stable, background for $t\in[\pi/\omega,2\pi/\omega]$ would be given by $\phi[(2\pi/\omega)-t]$. In addition to the growing stable background, which encroaches upon the droplets of the metastable phase during the second half-period, we assume that droplets of the stable phase nucleate and grow within the shrinking metastable droplets as depicted in Fig. 5(c). Furthermore, we assume that this nucleation and growth process is also described by Avrami's law, with the shrinking metastable phase analogous to the metastable background filling the entire system for $t\in[0,\pi/\omega]$. The complete prescription for the volume fraction of the growing stable background for $t\in[\pi/\omega,2\pi/\omega]$ is then

$$\phi'(t)\approx\phi\left(\frac{2\pi}{\omega}-t\right)+[(\text{shrinking metastable phase})\times(\text{growing stable phase inside shrinking droplets})]$$

$$=\phi\left(\frac{2\pi}{\omega}-t\right)+\left[1-\phi\left(\frac{2\pi}{\omega}-t\right)\right]\left[1-\phi\left(t-\frac{\pi}{\omega}\right)\right]$$

$$=1-\phi\left(t-\frac{\pi}{\omega}\right)\left[1-\phi\left(\frac{2\pi}{\omega}-t\right)\right]. \tag{5.4}$$

Thus the theoretical result for the magnetization during an entire period of $H(t)$ is

$$m(t)\approx\begin{cases}2\phi(t)-1, & 0<t<\pi/\omega\\ 2\phi'(t)-1=1-2\phi\left(t-\frac{\pi}{\omega}\right)\left[1-\phi\left(\frac{2\pi}{\omega}-t\right)\right], & \pi/\omega<t<2\pi/\omega.\end{cases} \tag{5.5}$$

Note that, in this approximation $m(2\pi/\omega)=m(0)$ for all frequencies. Although it gives very good values for $\langle A\rangle$ at all frequencies and for $\langle B\rangle$ especially at low frequencies, it gives a continuous change in $\langle Q\rangle$ with $\omega$, with no sign of a dynamic phase transition.

It is possible to rewrite Eq. (5.3) for $\Phi(t)$ by making the substitution $H=H_0\sin(\omega t)$ and $H'=H_0\sin(\omega t_n)$. After tedious, but straightforward, algebra this gives

$$\Phi(H)=\frac{B(T)\Omega_2\nu^2H_0}{\omega^3}\int_0^H H'^3 e^{-\Xi_0(T)/H'}\left[\sqrt{1-\left(\frac{H'}{H_0}\right)^2}-2\sqrt{1-\left(\frac{H}{H_0}\right)^2}+\frac{1-\left(\frac{H}{H_0}\right)^2}{\sqrt{1-\left(\frac{H'}{H_0}\right)^2}}\right]dH'. \tag{5.6}$$

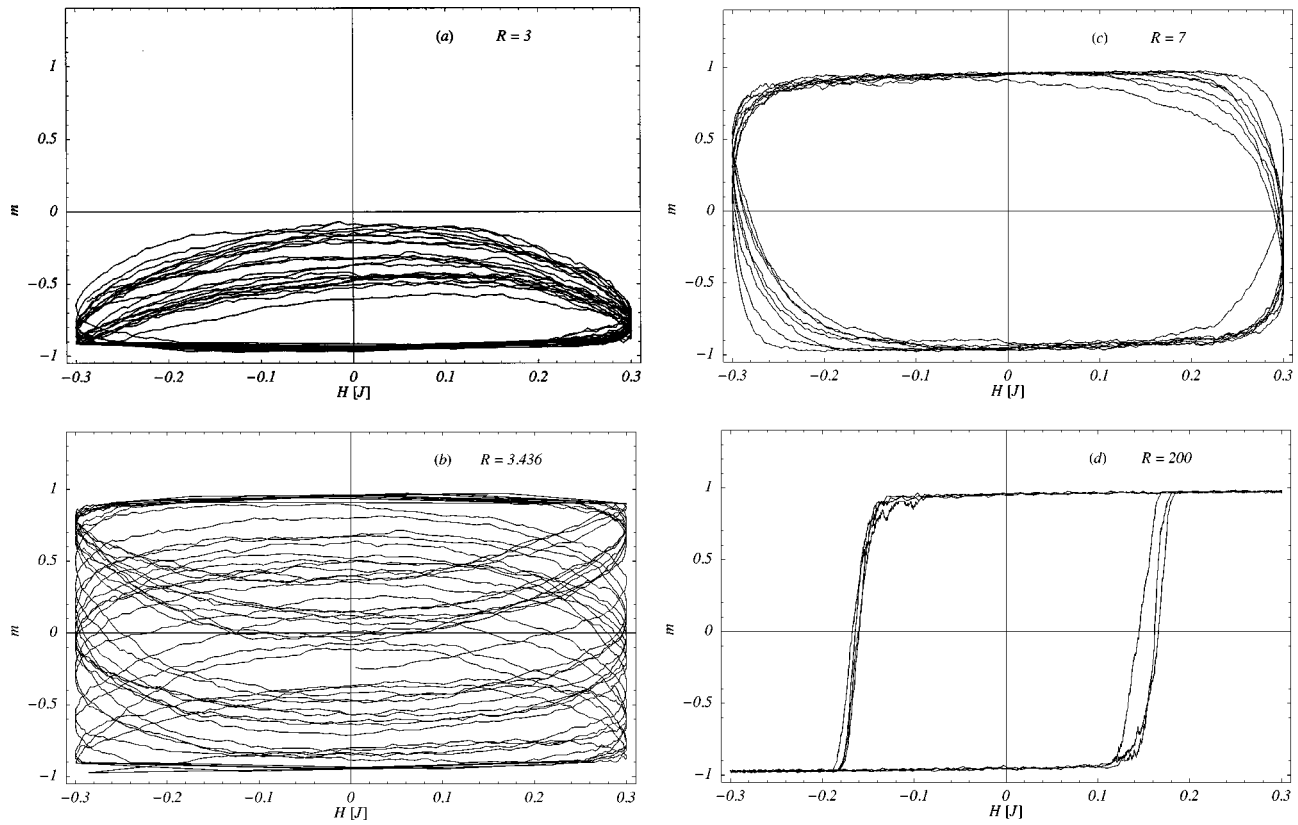


FIG. 6. Representative hysteresis loops obtained from Monte Carlo simulation data with system size $L=64$ for (a) $R=3$, (b) $R=3.436\approx R_{\mathrm{cr}}$, (c) $R=7$, and (d) $R=200$. Each panel shows loops for the same time intervals shown in the corresponding time-series data in Fig. 2.

The equation is valid for $H\in[0,H_0]$, so this expression allows a theoretical calculation of the magnetization for sufficiently low frequencies such that $m(t)$ completely switches sign within a *quarter* period of the field. Notice that $\omega$ is no longer part of the integration operation. A similar calculation has been used to describe experimental data for switching currents in (Nb,Co)-doped $BaTiO_3$ ceramics [13] and hysteresis loops for triglycine sulphate (TGS) single crystals [14,15] in the presence of an oscillating electric field. Those studies assume heterogeneous nucleation, and therefore obtain a frequency dependence of $\omega^{-d}$, rather than $\omega^{-(d+1)}$ [see Eq. (5.6)] for the case of homogeneous nucleation studied here. The integral in Eq. (5.6) is evaluated *once* for $H\in[0,H_0]$, from which $m(t)$ for $t\in[0,\pi/(2\omega)]$ at any frequency can be calculated. For numerical reasons, Eq. (5.6) enables the theoretical prediction of the hysteretic response to be more easily calculated for lower frequencies than by using Eq. (5.3) alone. The values of $m(t)$ obtained from both Eq. (5.3), for intermediate to high frequencies, and Eq. (5.6), for low frequencies, are used in calculating the theoretical predictions for $\langle A\rangle$ and $\langle B\rangle$ in Sec. VI.

## VI. HYSTERESIS-LOOP AREAS AND CORRELATION

In this section we calculate the hysteresis-loop area $A$ and the correlation between the field and the system magnetization $B$, defined in Eqs. (1.3) and (1.4), respectively. These quantities are calculated over each period in the entire time series. From the resulting ''filtered'' time series we construct histograms to obtain the probability densities of $A$ and $B$ for each separate frequency of the field. The hysteresis-loop area represents the energy dissipated during a single period of the field [2–4]. It is therefore one of the most important physical quantities characterizing hysteretic systems, and it is frequently measured in experiments.

Recent experiments on ultrathin ferromagnetic films [32,33], as well as numerical simulations of two-dimensional Ising models [35,62,66,88], have been interpreted in terms of a low-frequency power law $A\propto H_0^a\omega^b$, with a range of exponent values reported [62,66,88]. This interpretation is not fully consistent with the fluctuation-free mean-field result [54,56], $A=A_0+\mathrm{const}\times[\omega^2(H_0^2-H_{\mathrm{sp}}^2)]^{1/3}$ with positive constants $A_0$ and $H_{\mathrm{sp}}$, which has been applied to analyze experiments on ultrathin films of Co on Cu(001) [37]. Nor does the single power-law dependence agree with the logarithmic dependence expected if thermally activated nucleation [11,29,35,68] is the rate-determining process. Here we present in detail analytical and numerical results that indicate a resolution of this puzzling situation. A brief summary of some of the results was given in Ref. [52].

The hysteresis loops depend on frequency and have qualitatively different shapes above, near, and below the dynamic phase transition. Figure 6 shows plots of the magnetization vs field in the MD regime for four field frequencies. The loops shown here are for the same frequencies as the time series shown in Fig. 2. The loops shown in Fig. 6(b) indicate the large fluctuations in the average magnetization near the transition at $R=3.436\approx R_{\mathrm{cr}}$. As the frequency is moved further away from the transition, the variation in the loops be-

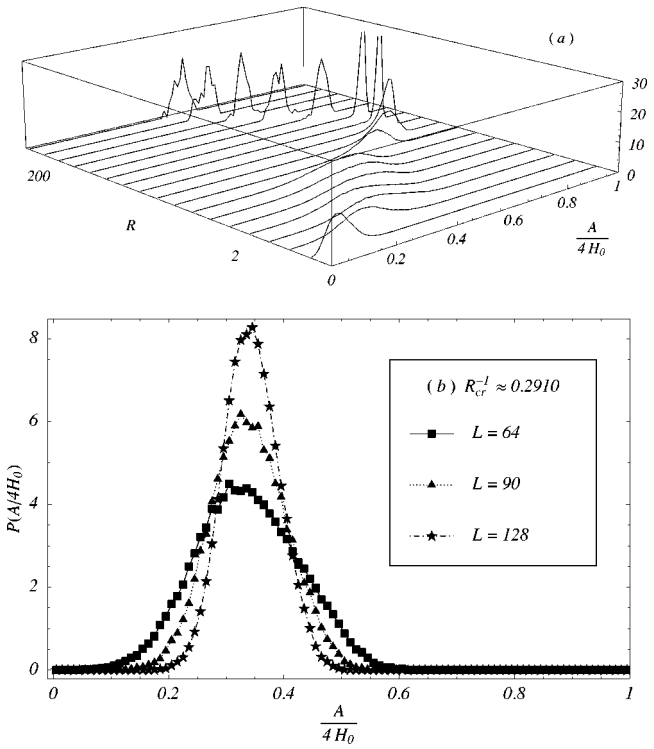


FIG. 7. Probability densities of the hysteresis-loop area $A=-\oint m(H)dH$. The loop area has been normalized by the maximum possible loop area $4H_0$. (a) $L=64$. The values of the scaled period shown are $R=2$, 3, $3.436\approx R_{\rm cr}$, 3.5, 3.75, 3.9, 4, 5, 6, 7, 8.4, 12, 25, 50, 80, 140, and 200, so the $R$ axis is not linear. The two $R$ values explicitly marked indicate the directions of increasing and decreasing frequency. (b) Distributions near the critical frequency shown for $L=64$, 90, and 128. The distributions are narrower away from $R_{\rm cr}$ but look qualitatively similar.

comes smaller. The loops for a very low frequency, $R=200$ in Fig. 6(d), show how the magnetization reverses sign early in each half-period of the field, saturating close to the equilibrium magnetization at a field well below $H_0$. The low-frequency approximations for $A$ derived later in this section are applicable to these squarish loops, in which the switching field is small and the field variation is nearly linear.

Probability densities for $A$ are shown in Fig. 7. The loop area has been divided by the maximum possible loop area $4H_0$. Figure 7(a) shows the probability densities for $L=64$ and several values of $R$ between $R=2$ and 200. In contrast to the SD regime [50], the distributions are unimodal for *all* frequencies. The roughness of the distributions at the lowest frequencies is due to the lack of statistics because the time series for these frequencies contain a smaller total number of periods than the data for the intermediate and high frequencies. Figure 7(b) shows the probability densities for a frequency near the transition for $L=64$, 90, and 128. The position of the peak for each of these distributions appears to be independent of system size. However, the width of the distribution becomes smaller with increasing system size. This observation is consistent with the system-size dependence of the switching-field distribution in field-reversal experiments [26]. For further details on the $L$ dependence of the width near the transition, see the end of Sec. VII. The average loop area for a specific frequency is a quantity often displayed in

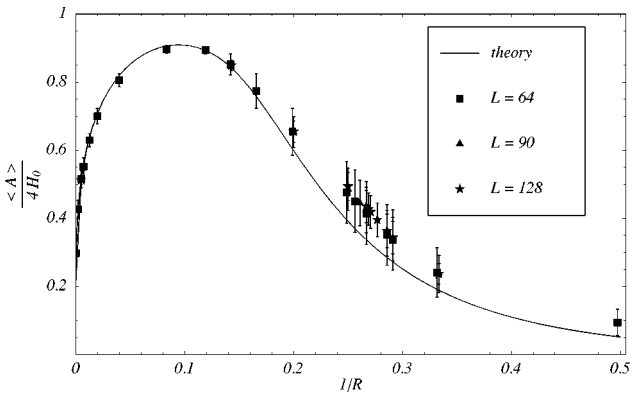


FIG. 8. Mean and standard deviation of the loop-area distributions vs the scaled frequency $1/R$. The data points are the means of the distributions shown in Fig. 7 for $L=64$ along with the means of the corresponding distributions for $L=90$ and 128. The vertical bars are *not* error bars, but give the standard deviations of those distributions. The solid curve comes from numerical integration of Eq. (1.3) using the values of $m(t)$ from Sec. V. The single free parameter $B(T)$ is adjusted so the theoretical prediction agrees with the data point at $1/R=0.005$, as described in the text.

experimental and numerical studies of hysteresis. It can also be obtained in the present case, and we do so below. The means of the distributions in Fig. 7(a) are shown in Fig. 8, along with the average loop areas for $L=90$ and 128. The solid curve in Fig. 8 is obtained by numerical integration of Eq. (1.3) using the values of $m(t)$ obtained in Sec. V.

For any finite time series there is a sufficiently low frequency such that the magnetization switches during every half-period of the field. For very low frequencies the magne-

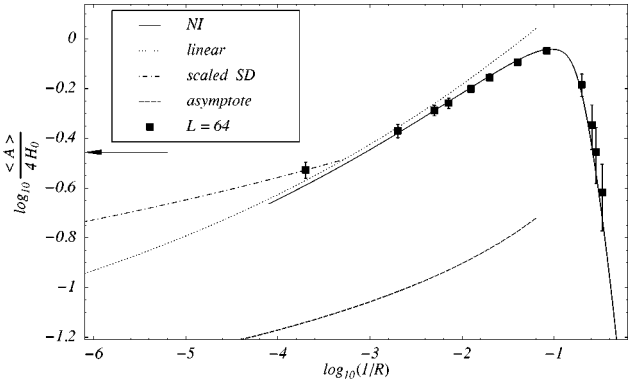


FIG. 9. Log-log plot for the mean of the loop-area distributions vs the scaled frequency $1/R$. The vertical bars are *not* error bars, but give the standard deviations of those distributions. The data points are the same as those used for $L=64$ in Fig. 8 for the lowest frequencies. The solid curve (*NI* for numerical integration) is the same as the solid curve in Fig. 8. (Due to numerical difficulties, this calculation was not extended to lower frequencies than those shown.) The dotted curve results from numerical solution of the linear approximation [Eq. (6.3)]. The dash-dotted curve is the prediction for the loop area in the SD regime for $L=64$, scaled so that it may be plotted along with the MD results. The dashed curve is the asymptotic, logarithmic frequency dependence for the MD loop area [Eq. (6.9)]. This asymptotic result approaches the full solution only for frequencies that are lower than the crossover to the SD solution, even for very large $L$. The arrow indicates the area of a hysteresis loop with $H_{\rm s}\approx H_{\rm DSP}(L=64)$.

tization switches *before* the field reaches its extreme value during every half-period. In this frequency regime, $m(t)$ switches sign abruptly relative to the length of a field period [see Fig. 2(d)]. The switching time $t_s$ may be found by solving $m(t_s)=0$. Thus the equation for $t_s$ becomes

$$\ln 2=\Phi(t_s). \tag{6.1}$$

As Figs. 2(d) and 6(d) show, for sufficiently low frequencies $m(t)$ switches sign early in the period, i.e. at a value $|H(t)|<H_0$. This allows the approximation $H(t)\approx H_0\omega t$ to be used for the field, henceforth referred to as ''the linear approximation in the field.'' Using this approximation and the substitutions $x=H_0\omega t$ and $x'=H_0\omega t_n$ allows Eq. (5.3) to be rewritten as

$$\Phi(t_s)\approx\frac{B(T)\Omega_2\nu^2}{4H_0^3\omega^3}\int_0^{H_s}x'^3(x^2-x'^2)^2\exp\left[-\frac{\Xi_0(T)}{x'}\right]dx'=\frac{B(T)\Omega_2\nu^2}{4H_0^3\omega^3}\left\{x^4\int_0^{H_s}x'^3\exp\left[-\frac{\Xi_0(T)}{x'}\right]dx'\right.$$
$$\left.-2x^2\int_0^{H_s}x'^5\exp\left[-\frac{\Xi_0(T)}{x'}\right]dx'+\int_0^{H_s}x'^7\exp\left[-\frac{\Xi_0(T)}{x'}\right]dx'\right\}, \tag{6.2}$$

where $H_s=H_0\omega t_s$. Together with Eq. (6.1), this yields the equation for $H_s$,

$$\ln 2=\frac{B(T)\Omega_2\nu^2}{4H_0^3\omega^3}\left\{H_s^4\Xi_0^4(T)\Gamma\left[-4,-\frac{\Xi_0(T)}{H_s}\right]-2H_s^2\Xi_0^6(T)\Gamma\left[-6,-\frac{\Xi_0(T)}{H_s}\right]+\Xi_0^8(T)\Gamma\left[-8,-\frac{\Xi_0(T)}{H_s}\right]\right\}, \tag{6.3}$$

where each of the integrals in Eq. (6.2) has been rewritten as an incomplete gamma function [89] using the expression

$$\int_0^x u^n e^{-a/u}du=a^{n+1}\Gamma\left[-(1+n),\frac{a}{x}\right]. \tag{6.4}$$

For small $\omega$ the hysteresis loops are practically square, so the scaled loop area in the low-frequency (LF) limit can be expressed as

$$\frac{\langle A\rangle_{LF}}{4H_0}\approx m_{eq}\frac{H_s(\omega)}{H_0}. \tag{6.5}$$

The switching field $H_s(\omega)$ is obtained by numerical solution of Eq. (6.3), and the result for $\langle A\rangle_{LF}/4H_0$ is shown as the dotted curve in Fig. 9. There is good agreement between this linear approximation calculation, the numerical integration calculation, and the MC data for low frequencies. The slight overestimate of the loop area by the linear approximation at low frequencies is due to a systematic error in the way that the loop area is calculated from the value of $H_s(\omega)$. The disagreement near the maximum in the loop area is due to the breakdown of the linear approximation as the magnetization begins to switch sign only at fields close to $H_0$.

The dash-dotted curve in Fig. 9 is the theoretical low-frequency prediction for $L=64$ in the SD regime. This curve corresponds to the solid curve in Fig. 11(b) of Ref. [50], appropriately rescaled so that it may be shown together with the MD results. This re-scaling consists of using $H_0=0.3J$ in the quantity $A/4H_0$ and $\langle\tau(H_0)\rangle$ for the MD regime in calculating the scaled frequency $1/R$. The MC data point at the very lowest frequency in Fig. 9 ($R=5000$) agrees with the SD, rather than the MD, theoretical prediction, even though the simulation was performed with $H_0=0.3J$. This crossover from MD to SD hysteretic behavior is a completely frequency-dependent effect. As the frequency of the field decreases, the value of the switching field $H_s(\omega)$ decreases as well. For sufficiently low frequencies that $H_s(\omega)<H_{DSP}(L,T)$, the system undergoes SD decay before the field becomes large enough to produce MD decay. In fact, the intersection of the SD and MD theoretical predictions occurs at a value of $A$ which corresponds to a square loop with a switching field of $H_s(\omega)\approx H_{DSP}(L,T)$. While $m(t)$ and $A$ do not depend on system size in the MD regime, $A$ in the SD regime, and hence the location of the crossover, depends on $L$ through the $L^{-d}$ dependence of the lifetime in the SD regime [see Eqs. (4.15) and (7.13) of Ref. [50]].

One can obtain an approximate analytic solution for $\langle A\rangle_{LF}$ by taking the first three terms in the asymptotic expansion [89]

$$\Gamma(a,x)\sim x^{a-1}e^{-x}\left[1+\frac{a-1}{x}+\frac{(a-1)(a-2)}{x^2}+\cdots\right] \tag{6.6}$$

for large $x$. Straightforward, but lengthy, algebra gives the following asymptotic expansion for Eq. (6.3):

$$\left(\frac{H_s}{\Xi_0(T)}\right)^{11}\exp\left[-\frac{H_s}{\Xi_0(T)}\right]\approx(DH_0\omega)^3, \tag{6.7}$$

where we define

$$D=\left(\frac{\ln 2}{2B(T)\Omega_2\nu^2\Xi_0^8(T)}\right)^{1/3}. \tag{6.8}$$

With $B(T)=0.02048J^{-3}$ MCSS$^{-1}$ and the values found in Table I this gives $D=17.905J^{-1}$ MCSS$^{-1}$. Ignoring the nonexponential prefactor in Eq. (6.7), solving for the switching field $H_s(\omega)$, and substituting it into Eq. (6.5) results in the asymptotic, logarithmic frequency dependence for the loop area,

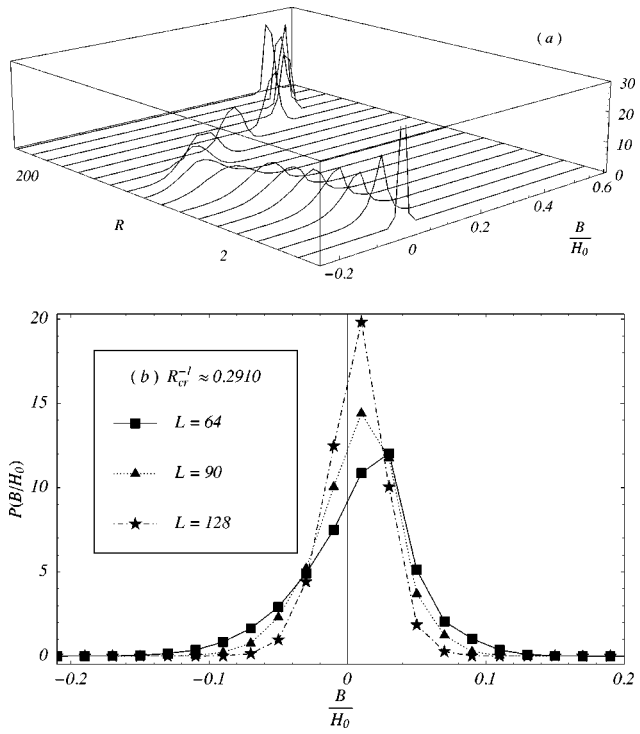


FIG. 10. Probability densities of the correlation, $B=(\omega/2\pi)\oint m(t)H(t)dt$. (a) $L=64$. The values of $R$ shown are the same as in Fig. 7. (b) Distributions near the critical frequency shown for $L=64$, 90, and 128. Lines connecting the data points are guides to the eye. The distributions look qualitatively similar, even away from $R_{\rm cr}$.

$$\langle A\rangle_{\rm LF}\approx\tfrac{4}{3}\Xi_0(T)[-\ln(DH_0\omega)]^{-1}. \tag{6.9}$$

As in the SD case [50,52], from a log-log plot of the loop area versus frequency one can extract effective exponents from the data over nearly two decades in $1/R$. However, these effective exponents depend strongly on the frequency range in which the fit is performed. Very small effective exponents that appear consistent with this picture were recently reported by Suen *et al.* for ultrathin Co films on Cu(001) [38].

As for the SD regime, we stress that the asymptotic low-frequency behavior described by Eq. (6.9) would only be seen for *extremely* low frequencies, where the dotted and dashed curves in Fig. 9 come together. Therefore, due to the dependence of $H_{\rm DSP}$ on $L$ the crossover to SD droplet behavior will occur at frequencies much larger than those for which this asymptotic expression is valid even for large $L$. For a system size of $L=10^9$ the ratio of the full numerical solution to the asymptotic expression is approximately two near the crossover frequency, which for that system size would be near $1/R\approx 6\times 10^{-9}$.

Relatively few studies have considered $B$, the correlation of the magnetization with the external field. Our theoretical derivations of $B$ are analogous to those for $A$. The probability densities of $B$ in the MD regime are shown in Fig. 10. Figure 10(a) shows the probability densities for several values of $R$ between 2 and 200. The source of the roughness of the distributions at the lowest frequencies is the same as in Fig. 7(a). Figure 10(b) shows the probability densities for a frequency near the transition for $L=64$, 90, and 128. The system-size dependence of the peak position and the width of the distributions is similar to that for the loop-area distributions. The means of the distributions in Fig. 10(a) are shown in Fig. 11 along with the results for $L=90$ and 128. The solid curve is obtained by numerical integration of Eq. (1.4) similar to the procedure for $A$. The agreement between the MC data and the theoretical prediction is very good for low and high frequencies, but poor for intermediate frequencies, where the MC data take on negative values. This disagreement is probably due to the procedure for calculating $m(t)$ during a half-period in which shrinking droplets are present in the system (see Sec. V).

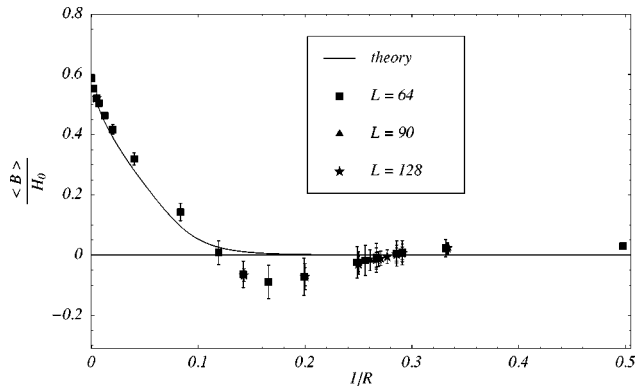


FIG. 11. Mean and standard deviation of the correlation distributions vs the scaled frequency $1/R$. The data points are the means of the distributions shown in Fig. 10(a) for $L=64$, along with the corresponding results for $L=90$ and 128. The vertical bars are *not* error bars, but give the standard deviations of the distributions. The solid curve comes from a theoretical calculation analogous to that in Fig. 8.

As for the SD regime [50], the physical significance of the integrals $A$ and $B$ can be clarified by comparison with linear response theory. One can easily find that $A/(\pi H_0^2)$ and $2B/H_0^2$ correspond to the dissipative and reactive parts of the complex linear response function, respectively. It is therefore natural to combine $A$ and $B$ into an analogous *nonlinear* response function

$$\hat{X}(H_0,T,\omega)=\frac{1}{H_0^2}\left[2B+\frac{i}{\pi}A\right]. \tag{6.10}$$

The frequency dependence of the norm of this response function, $|\hat{X}|$, is shown in Fig. 12. The maximum in $A$ (Fig. 8) and the sign change in $B$ (Fig. 11), which occur close together in frequency, are characteristic behaviors of dissipative and reactive parts of a response function near resonance. The behavior of $\langle A\rangle$ and $\langle B\rangle$ in this frequency range is very similar to that observed in the SD regime [50], where we associate it with stochastic resonance [90]. Whether or not this name is appropriate for the low-frequency synchronization of $m(t)$ with $H(t)$ in the MD regime is probably a matter of taste. Although the overall fluctuations in $m(t)$ are small, the switching is entirely driven by random nucleation on a microscopic scale.

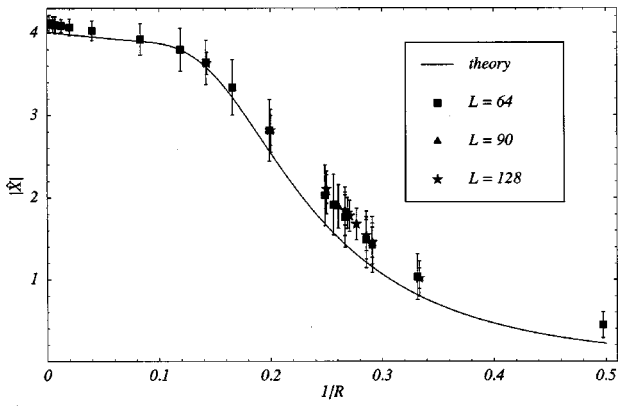


FIG. 12. Mean and standard deviation of the norm of the response function $|\hat{X}|$ vs the scaled frequency $1/R$. The data points are obtained using the loop-area and correlation data in Figs. 8 and 11. The solid curve is obtained using the theoretical values for $\langle A\rangle$ and $\langle B\rangle$ in those figures.

## VII. DYNAMIC PHASE TRANSITION

Although nonequilibrium phase transitions have been studied for over two decades, the understanding of their universality and scaling properties remains much weaker than for equilibrium critical phenomena. Finite-size scaling is routinely used to determine the location and critical exponents of equilibrium thermodynamic phase transitions from numerical results for finite systems [72,91]. A true phase transition occurs only in the thermodynamic limit, i.e., as the system size approaches infinity while the energy and particle densities are kept constant. For simulations on finite systems, quantities such as the susceptibility and specific heat only display a bounded peak, rather than a divergence, as a function of temperature or field. However, for simulations performed on larger and larger lattices, thermodynamic quantities approach the infinite-size limit. It is this approach to the thermodynamic limit that is utilized to obtain estimates of the critical exponents from various system sizes.

Second-order phase transitions in equilibrium systems are characterized by a set of critical exponents, each of which describes the behavior of a different quantity at the critical point. Three of these quantities and their associated exponents are [92] the order parameter ($M\sim|\bar{t}|^{\beta}$ for $\bar{t}<0$), the susceptibility ($\chi\sim|\bar{t}|^{-\gamma}$), and the correlation length ($\xi\sim|\bar{t}|^{-\nu}$), where $\sim$ denotes ''the singular behavior of.'' The field conjugate to the order parameter is understood to be zero, and $\bar{t}=(T-T_c)/T_c$ is the reduced temperature. Finite-size scaling theory allows one to estimate the critical exponents by measuring the system-size dependence of various quantities. Combining the expression for the correlation length exponent with the finite-size scaling assumption, $\xi(T_c(L))\sim L$, gives

$$|T_c(L)-T_c|\propto L^{-1/\nu}, \tag{7.1}$$

where $T_c(L)$ can be defined as the location of the peak in the susceptibility for a given $L$ [72,91]. When combined with the definitions for the critical exponents, Eq. (7.1) gives

$$\chi_L^{\text{peak}}\propto L^{\gamma/\nu} \tag{7.2}$$

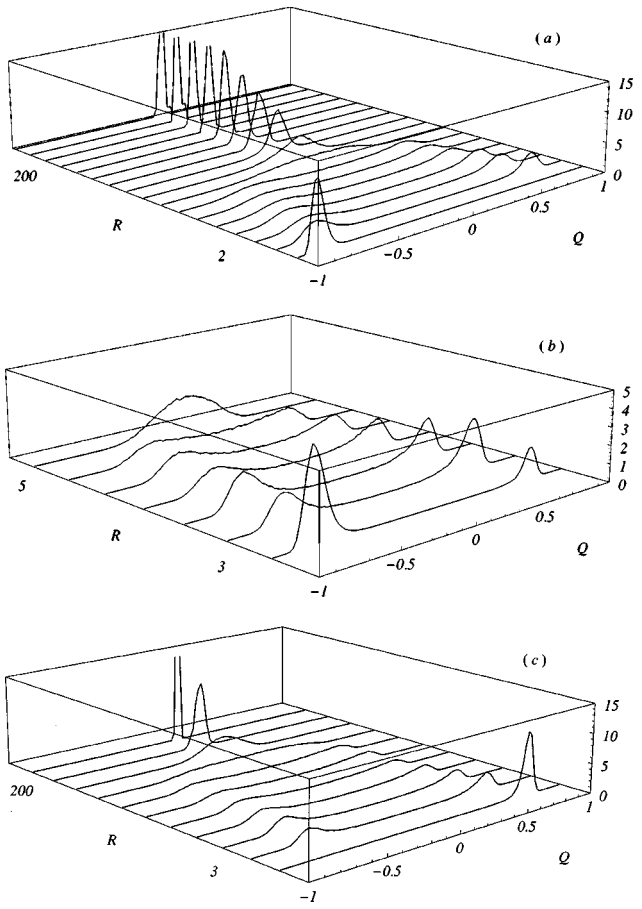


FIG. 13. Probability densities of the period-averaged magnetization $Q=(\omega/2\pi)\oint m(t)dt$. (a) $L=64$. The values of $R$ shown are the same as in Fig. 7. (b) $L=90$. The values of the scaled period shown are $R=3, 3.436\approx R_{\text{cr}}$, 3.5, 3.75, 3.835, 4, and 5. (c) $L=128$. The values of the scaled period shown are $R=3, 3.436\approx R_{\text{cr}}$, 3.5, 3.612, 3.693, 3.721, 3.75, 4, 5, 7, and 200. The unimodal distributions for the smallest $R$ value in (a) and (c) are due to the finite simulation time.

and

$$\langle|M|^n\rangle_L\propto L^{-n(\beta/\nu)}, \tag{7.3}$$

where $\chi_L^{\text{peak}}$ is the maximum value of the susceptibility for a given $L$, and $\langle|M|^n\rangle_L$ is the $n$th moment of the norm of the order-parameter at $T_c$.

The period-averaged magnetization $Q$ has been proposed as a ''dynamic order parameter'' for systems exhibiting hysteresis [55,57–62,69]. Those studies of the Ising model have suggested the existence of a dynamic phase transition between an ordered dynamic phase with $\langle|Q|\rangle>0$ and a disordered dynamic phase with $\langle|Q|\rangle\approx 0$. Figure 13 shows the probability densities of $Q$ in the MD regime for $L=64$, 90, and 128. For each system size, as the frequency of $H(t)$ decreases, the probability densities for $Q$ change from bimodal distributions with the two peaks each centered around a nonzero value of $Q$, to unimodal distributions with a peak around $Q=0$. Each of the $Q$ distributions shown in the three-dimensional Fig. 13 is a histogram of $Q$ time-series values (see Fig. 3) at a particular frequency. These distributions suggest the presence of a second-order dynamic phase tran-

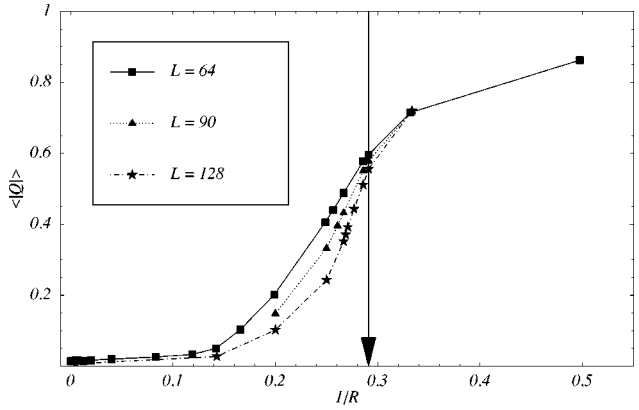


FIG. 14. Mean of the norm of the period-averaged magnetization vs the scaled frequency $1/R$. The finite-size effects are clearly seen for frequencies in the neighborhood of the dynamic phase transition. The arrow indicates the approximate value of the critical frequency $1/R_{\mathrm{cr}}$. Lines connecting the data points are guides to the eye.

sition. In particular, the frequency dependence for these probability densities is strikingly similar to the dependence on inverse temperature for probability densities of the equilibrium magnetization in the zero-field Ising model. We therefore identify the norm of the period-averaged magnetization, $|Q|$, as the order parameter of the dynamic phase transition, and we apply finite-size scaling theory in analogy to the scaling theories used to quantify second-order phase transitions in *equilibrium* systems. Figure 14 shows the average norm of the period-averaged magnetization, $\langle|Q|\rangle$, for the same system sizes as in Fig. 13. This figure clearly suggests a DPT as the average order parameter $\langle|Q|\rangle$ changes from a value near zero to a nonzero value. Rather than a sudden change in the order parameter, the transition region is ''smeared'' out due to finite-size effects. The mean and standard deviation for $|Q|$ are system-size dependent as well. We quantify these finite-size effects below.

At a second-order phase transition there is a divergence in the susceptibility. For equilibrium systems, the fluctuation-dissipation theorem relates the susceptibility to fluctuations in the order parameter. For the present system, it is not obvious what the field conjugate to $Q$ might be. Therefore, we cannot measure the susceptibility directly. However, we can calculate the variance in $|Q|$ as a function of frequency and study its system-size dependence. We define $X$ as

$$X = L^2\,\mathrm{Var}(|Q|) = L^2[\langle Q^2\rangle - \langle|Q|\rangle^2]. \tag{7.4}$$

If the system were to obey a fluctuation-dissipation relation, $X$ would be proportional to the susceptibility, and both would scale with $L$ in the same manner. Figure 15 shows $X$ vs $1/R$ for all three system sizes. For all three values of $L$, $X$ displays a prominent peak near the transition frequency, which increases in height with increasing $L$, while no finite-size effect is seen at lower and higher frequencies. This finite-size effect in $X$ implies the existence of a divergent length associated with the order-parameter correlation function near the dynamic transition. The observation that $P(|Q|)$ displays no peak near $|Q|=0$ in the ordered dynamic phase is additional evidence of the second-order (as opposed to first-order) nature of this transition [93].

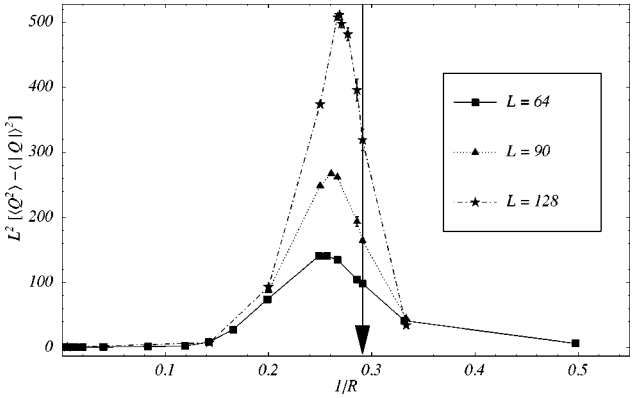


FIG. 15. Order-parameter fluctuation $X = L^2\,\mathrm{Var}(|Q|)$ vs the scaled frequency $1/R$. The ''disordered dynamic phase'' ($\langle|Q|\rangle \approx 0$) lies on the low-frequency side of the peaks. The ''ordered dynamic phase'' ($\langle|Q|\rangle > 0$) lies on the high-frequency side. The statistical error bars are estimated by partitioning the data into ten blocks. Error bars smaller than the symbol sizes are not shown. The arrow indicates the approximate value of the critical frequency $1/R_{\mathrm{cr}}$. Lines connecting the data points are guides to the eye.

The cumulant intersection method [72,91] is useful for determining the location of a second-order transition when the critical exponents are not known. In order to estimate the location of the transition we define the ''dynamic'' fourth-order cumulant ratio

$$U_L = 1 - \frac{\langle|Q|^4\rangle_L}{3\langle|Q|^2\rangle_L^2}, \tag{7.5}$$

where $\langle|Q|^n\rangle = \int_0^\infty |Q|^n P(|Q|)\,d|Q|$. Figure 16 shows $U_L$ vs $1/R$ for the same system sizes shown in Fig. 15. Above the transition frequency, in the $\langle|Q|\rangle > 0$ ordered dynamic phase, $U_L$ approaches $\frac{2}{3}$, corresponding to two narrow peaks centered at $\pm\langle|Q|\rangle$. Below the transition frequency, in the $\langle|Q|\rangle \approx 0$ disordered dynamic phase, $U_L$ approaches 0, corresponding to a Gaussian centered at zero. At the transition, the cumulant should have a nontrivial fixed value $U^*$. Therefore, the location of the cumulant intersection gives an estimate of the transition frequency without foreknowledge

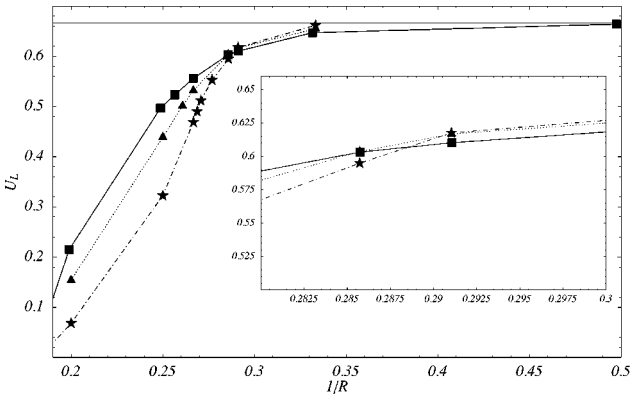


FIG. 16. Fourth-order cumulant ratio $U_L$ vs scaled frequency $1/R$, for $L = 64$, 90, and 128. We use the same symbols as in Fig. 15. The horizontal line marks $U_L = \frac{2}{3}$. Lines connecting the data points are guides to the eye. Inset: area close to the cumulant crossing at $1/R_{\mathrm{cr}} \approx 0.2910$.

of the critical exponents. Due to the large spacing of our data and possible correction-to-scaling effects, we cannot identify a unique intersection point. We estimate the location of the intersection by the crossing for the two largest system sizes near $R_{\rm cr}^{-1}\approx 0.2910$ ($R_{\rm cr}\approx 3.436$) with $U_L = U^* \approx 0.61$. This is close to an extremely precise transfer-matrix calculation of $U^* = 0.610\,690\,1(5)$ [94] as well as MC estimates [95] for the two-dimensional Ising model in equilibrium. However, as recently pointed out by Luijten, Binder, and Blöte [96], the value of the cumulant intersection should not be taken too seriously unless a sufficient range of system sizes is available.

With our estimate for the transition frequency, we can now approximate the critical exponents $\beta$, $\gamma$, and $\nu$ characterizing the transition by using Eqs. (7.1)–(7.3), replacing $T_c$ by $R_c$, $\chi_L^{\rm peak}$ by $X_L^{\rm peak}$, and $\langle |M|^n \rangle_L$ by $\langle |Q|^n \rangle_L$. To extract exponent estimates using these relations, we use a method sometimes referred to as ''phenomenological renormalization'' [91] of the MC data. This method consists of estimating an exponent by using two system sizes, $bL$ and $L$. The following example is a derivation of an exponent estimate for $\beta/\nu$:

$$\frac{\langle |Q|^n \rangle_{bL}}{\langle |Q|^n \rangle_L} \propto \frac{(bL)^{-n(\beta/\nu)}}{L^{-n(\beta/\nu)}} = b^{-n(\beta/\nu)},$$

which yields

$$-\ln\left[\frac{\langle |Q|^n \rangle_{bL}}{\langle |Q|^n \rangle_L}\right] \Big/ \ln b = n\left(\frac{\beta}{\nu}\right) + {\rm O}(1/\ln b). \qquad (7.6)$$

Similar relations can be found for the other exponent ratios:

$$\ln\left[\frac{X_{bL}^{\rm peak}}{X_L^{\rm peak}}\right] \Big/ \ln b = \frac{\gamma}{\nu} + {\rm O}(1/\ln b), \qquad (7.7)$$

$$\ln\left[\frac{|R_c(bL) - R_c|}{|R_c(L) - R_c|}\right] \Big/ \ln b = \frac{1}{\nu} + {\rm O}(1/\ln b). \qquad (7.8)$$

In the large-system limit these exponent estimates will be linear when plotted vs $(\ln b)^{-1}$. Then one can extrapolate to the infinite-size limit by performing a linear fit of the data to find the intercept at $(\ln b)^{-1} = 0$. Simulations with larger system sizes would be computationally prohibitive, and smaller system sizes would no longer be in the MD regime. With data for only three system sizes, the exponent estimates obtained using the two largest system sizes are easily shown to be identical to those obtained using the extrapolation procedure above. We calculate two sets of estimates for $\beta/\nu$, one using the scaling relation for the second moments of the order-parameter distribution ($n=2$) and the other using $n=4$, obtaining $(\beta/\nu)_{n=2} \approx 0.111$ and $(\beta/\nu)_{n=4} \approx 0.113$. Our estimates for the other exponents are $\gamma/\nu \approx 1.84$ and $\nu \approx 1.1$. Also, we obtained an independent estimate for the exponent $\nu$ by measuring the finite-size effects in the location of the high-frequency zero crossing in $\langle B \rangle$. The estimate obtained is $\nu \approx 1.09$, in good agreement with that obtained from the location of $X^{\rm peak}$. Our results are close to the two-dimensional Ising values for the analogous exponent ratios ($\beta/\nu = 1/8 = 0.125$, $\gamma/\nu = 7/4 = 1.75$, $\nu = 1$). Given the accuracy of our data however, our exponent estimates are also not inconsistent with the universality class of two-dimensional, random percolation ($\beta/\nu = 5/48 \approx 0.104$, $\gamma/\nu = 43/24 \approx 1.79$, $\nu = 4/3 \approx 1.33$). Combining the exponent estimates we find

$$2(\beta/\nu) + (\gamma/\nu) \approx 2.06 \approx d. \qquad (7.9)$$

This relation between the measured exponent ratios indicates the consistency of our scaling procedures, and thus strengthens our belief that the dynamic transition is a genuine, continuous phase transition. If the divergent length is indeed the correlation length that describes the order-parameter correlation function, then Eq. (7.9) is a hyperscaling relation. The DPT critical point then should be a nontrivial fixed point in the renormalization group sense. Based on the evidence presented in the following paragraph, we believe this is the case.

One should also consider the possibility that hyperscaling is violated and the DPT represents a mean-field critical point. The divergent length would then be the ''thermal length'' [72,96], whose divergence is governed by the exponent $(2\beta + \gamma)/d$. This would then be the exponent we have called ''$\nu$,'' and Eq. (7.9) would hold exactly as a tautology. However, our estimates for $\beta$ and $\gamma$ are far from those of a mean-field $\phi^4$ model ($\beta = \frac{1}{2}$ and $\gamma = 1$). Likewise, our estimated cumulant crossing, $U^* \approx 0.61$, is far from the expected mean-field value, $U^* = 1 - \Gamma^4(\frac{1}{4})/(24\pi^2) \approx 0.27$ [96,97]. Furthermore, if the phase transition were to be mean field in this two-dimensional system, it should have to be induced by some effective long-range interaction, which then should have the same effect in one dimension. However, exploratory MC simulations indicate that the one-dimensional Ising model in an oscillating field does not have a dynamic ordered phase [98]. The evidence summarized in this paragraph makes it extremely unlikely that hyperscaling is violated by the DPT.

The consistency of the estimates of $\nu$ from the positions of $X^{\rm peak}$ and the high-frequency zero crossing of $\langle B \rangle$ indicates that this zero probably occurs at the DPT. The two zeros of $\langle B \rangle$ are clearly separated in frequency, and our finite-size scaling results indicate that they remain so as $L \to \infty$. The low-frequency zero is associated with the maximum in $\langle A \rangle$. These observations enable us to answer the question recently raised by Acharyya [82] of whether the DPT corresponds to the maximum in $\langle A \rangle$. It does not.

To further illustrate the nature of the dynamic phase transition, the finite-size effects in the distributions for the norm of the order parameter, $|Q|$, are shown in Fig. 17. These probability densities for $|Q|$ are the symmetrized versions of selected distributions shown in Fig. 13. Distributions in the ordered dynamic phase region, i.e., above the transition frequency, should move toward a constant, nonzero value of $|Q|$ and become narrower with increasing $L$. This is seen in Fig. 17(a). For this frequency, the distribution of $Q$ for $L = 90$ is highly asymmetric about zero, and for $L = 128$ the distribution is unimodal. This gradual loss of symmetry with increasing $L$ is due to the finite length of the simulation time series, but it does not adversely affect our ability to analyze $P(|Q|)$. The distributions in Fig. 17(b) are in the disordered dynamic phase region, i.e., at a frequency slightly below the transition frequency. Due to finite-size effects, however, the distributions for $L = 64$ and 90 appear to be centered about nonzero values of $|Q|$. The distributions in Fig. 17(c) are

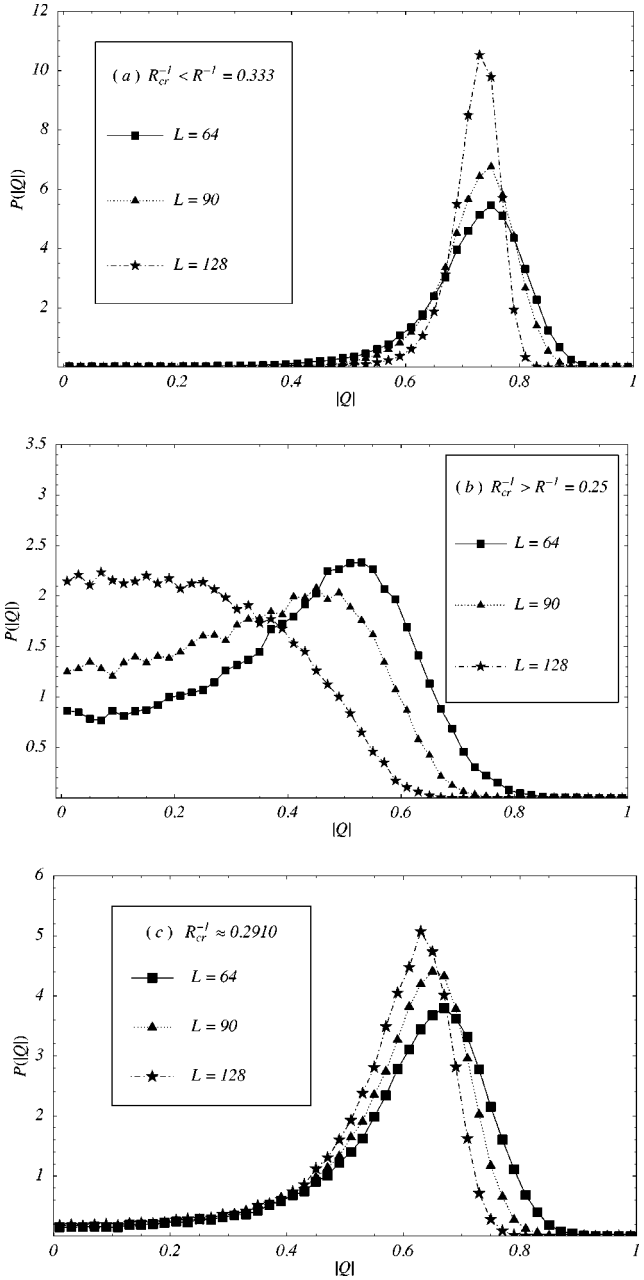


FIG. 17. Probability distributions for the norm of the period-averaged magnetization $|Q|$ for a frequency (a) above the transition, $1/R=0.333$; (b) below the transition, $1/R=0.25$; and (c) near the transition, $1/R=0.2910$. Lines connecting the data points are guides to the eye.

near the transition, and should scale with system size $L$. We assume that the mean of the order parameter scales with $L$, and define the scaling variable $\tilde{Q}=L^{\beta/\nu}|Q|$. Hence the scaled probability density for $|Q|$ is given by

$$\tilde{P}_L(\tilde{Q})=L^{-\beta/\nu}P(|Q|), \tag{7.10}$$

where the prefactor $L^{-\beta/\nu}$ ensures conservation of probability. Figure 18 shows this scaled probability density. The peak positions scale fairly well, the peak heights less so. This could be due to the following reasons. The frequency might be sufficiently far from the transition that single-parameter scaling is not adequate, and there might be corrections to the

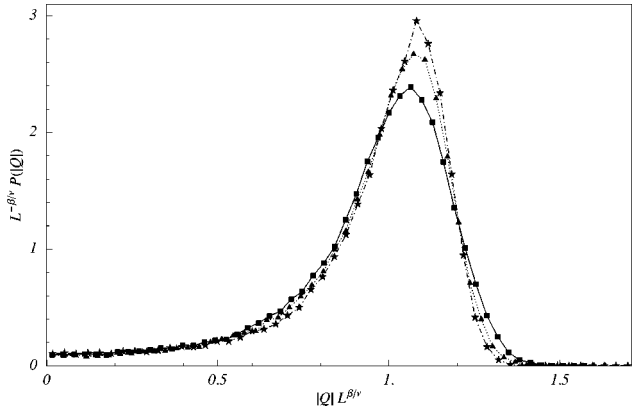


FIG. 18. Scaled probability densities of $|Q|$ for three system sizes. The same symbols are used as in Fig. 15. The scaling function is $L^{-\beta/\nu}P(|Q|)$ vs $L^{\beta/\nu}|Q|$, and the value of the scaling exponent used is $(\beta/\nu)_{n=2}\approx 0.11$. The scaled frequency of the field is $1/R=0.2910\approx 1/R_{\rm cr}$. Lines connecting the data points are guides to the eye.

finite-size scaling that are too large for these relatively small system sizes. Also, the lack of scaling for the peak heights could be due to the asymmetry in $P(Q)$ near the transition.

The results in this section clearly show that the statistical properties of the order parameter $Q$ exhibit finite-size scaling, and that scaling techniques developed for estimating the critical exponents for second-order phase transitions in equilibrium systems apparently can be successfully applied to estimate the exponents associated with the dynamic phase transition. While these scaling relations are concerned with $|Q|$, it is worth mentioning that one may also measure the fluctuations in the other two quantities measured, $A$ and $B$. Figure 19 shows the fluctuations for $A$ and $B$, defined in analogy to the order-parameter fluctuation $X$. The fluctuations in $A$ seem to show slight finite-size effects, as the peak positions appear to be approaching $R_{\rm cr}^{-1}$ with increasing $L$. One might speculate that this could indicate that $A$ is coupled to energy fluctuations which are logarithmically divergent, as they are for the two-dimensional Ising model in equilibrium. The fluctuations in $B$ show no significant finite-size effects.

## VIII. DISCUSSION

The mechanism by which a metastable phase decays depends sensitively on the system size, the temperature, and the strength of the applied field. For large systems and moderately strong fields, the decay proceeds through the nucleation and growth of *many* droplets of overturned spins in different parts of the system. This regime has been termed the multi-droplet (MD) regime. In this regime the magnetization response in a static field is described by the KJMA approximation (Avrami's law), which assumes the presence of many noninteracting, overlapping droplets. Theoretical predictions by a generalization of the KJMA approximation, in which a time-dependent nucleation rate and droplet interface velocity are used, agree well with simulations for quantities like the average hysteresis-loop area and correlation, especially at low driving frequencies. The time dependence is included in the theory by replacing the constant field $H$ by $H(t)=-H_0\sin(\omega t)$. This central idea provides the analytic

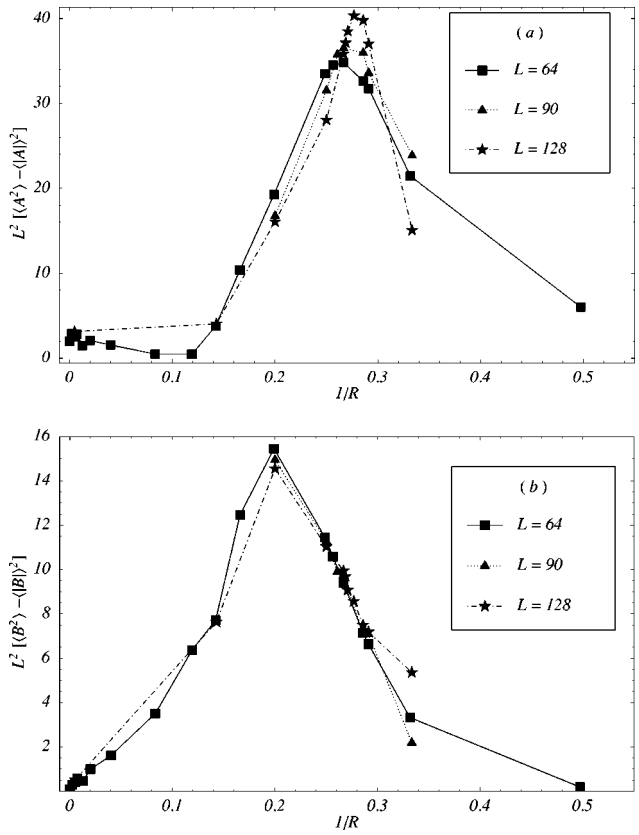


FIG. 19. (a) $L^2\mathrm{Var}(|A|)$ vs scaled frequency $1/R$. (b) $L^2\mathrm{Var}(|B|)$ vs scaled frequency $1/R$. In both parts, the lines connecting the data points are guides to the eye.

framework for our theoretical descriptions of quantities measured from the MC simulations in the MD regime. The theoretical calculations and the MC data agree very well, especially considering that only one adjustable parameter is needed, which was measured from a particular hysteresis simulation ($R=200$). All of the other constants used are either known from droplet theory or were measured for MC simulations of field reversal in kinetic Ising models. To the best of our knowledge, the work reported here is the first which explicitly considers hysteresis for the Ising model in the MD regime.

We compute the power spectral densities from the simulated time series, and qualitatively explain various features of the spectra in the full frequency range from the lowest observable frequencies to the rapid fluctuations due to thermal noise. For low field frequencies, the system is in the disordered dynamic phase, and the time series contain no large fluctuations. Consequently, the PSD's are flat at frequencies below the fundamental peak at the frequency of the field. The significant power density in the low-frequency portion of the PSD's corresponds to the long-time behavior in the filtered time series for $Q$. For high field frequencies, the system is in the ordered dynamic phase, and the time series display long-time behavior as the system switches between thermodynamic phases. This corresponds to a large power density in the low-frequency portion of the PSD's. Near the dynamic phase transition the PSD's exhibit similar behavior in the low-frequency part of the spectrum. Due to insufficiently long time series we are unable to resolve any quantitative difference between these PSD's and those in the ordered dynamic phase region.

We also calculate the hysteresis-loop area $A$ and the correlation $B$ for a wide range of frequencies. Because of its role as a measure of the energy dissipation in the system, $A$ is a quantity of particular experimental significance. For all frequencies, the loop-area and correlation distributions are unimodal due to the almost deterministic magnetization response in the MD regime. Our theoretical predictions for the frequency dependence of $\langle A\rangle$ and $\langle B\rangle$ use the time-dependent extension of Avrami's law to calculate $m(t)$, from which the loop area and correlation are calculated explicitly. The assumption is that the $m(t)$ values calculated for a *single* period accurately describe the average values of $A$ and $B$ over a long simulation time series. This assumption should be expected to break down most significantly for frequencies near the dynamic phase transition, where the fluctuations in the magnetization response are largest. This is clearly seen in Figs. 8 and 11, where the least satisfactory agreement between the theory and the MC data occurs for frequencies near the dynamic phase transition. For the low-frequency regime we obtain an analytic expression for $\langle A\rangle$. Our theoretical calculation agrees well with our MC results, and predicts an *extremely* slow crossover to a logarithmic dependence of the loop area on $H_0\omega$. The switching dynamics is dominated by nucleation, and indicates no overall power-law dependence for the loop area on field amplitude and/or frequency, in contrast to what has been claimed in other simulational and experimental studies. We emphasize that numerical analysis of data generated by our analytic solution, even over two or three frequency decades, could easily lead to the conclusion that the data were taken from a power law. Our simulations reveal that for frequencies *far* higher than those at which the asymptotic logarithmic dependence would be observable, a system-size-dependent crossover from MD to SD behavior occurs. This novel frequency dependence for $A$ is a consequence of the field dependence of the SD and MD decay mechanisms. As the frequency of the field becomes sufficiently small, the system is subject to fields smaller than $H_{\mathrm{DSP}}(T,L)$ for a sufficiently long time, so that SD decay usually occurs before the field becomes large enough for MD decay to happen.

The period-averaged magnetization $Q$ has been proposed as an order parameter associated with the dynamic phase transition (DPT) in kinetic Ising models. The DPT is a *nonequilibrium* phase transition which occurs due to an explicit time dependence in the Hamiltonian, rather than the dynamical rules governing the system. The probability densities that we obtain for $Q$ clearly show that the system changes from an ordered dynamic phase with nonzero $\langle |Q|\rangle$ to a disordered dynamic phase with $\langle |Q|\rangle \approx 0$ as the field moves from high to low frequencies. To distinguish this frequency-dependent change in $\langle |Q|\rangle$ as a true second-order phase transition rather than merely a simple bifurcation, we measure the finite-size effects at the DPT and apply finite-size scaling (FSS) techniques analogous to those used to measure the critical exponents which characterize *equilibrium* second-order transitions. The measured exponents ($\beta/\nu \approx 0.11$, $\gamma/\nu \approx 1.84$, and $\nu \approx 1.1$) are close to both the two-dimensional Ising and random percolation values, and they represent strong evidence that hyperscaling is obeyed. Our success in

applying FSS techniques borrowed from the theory of equilibrium second-order phase transitions to this nonstationary nonequilibrium problem suggests the possibility of mapping other suitably defined quantities for this system to thermodynamic entities, such as the field conjugate to the order parameter, the specific heat, and the correlation length. Such a nonequilibrium thermodynamic theory for steady states as been attempted by Paniconi and Oono [99].

In future work we plan to analyze longer simulations on larger system sizes to determine more accurately the values of the exponents and the location of the DPT. This includes measuring the possible finite-size effects in the probability distributions of the energy [65], which might be related to the finite-size effects seen in the fluctuations in *A*. If a fluctuation-dissipation theorem could be shown for this system, the order-parameter and energy fluctuations could be related to a nonequilibrium susceptibility and specific heat, respectively. Another important question left to future study is if and to what extent the exponents depend on the temperature and field amplitude. While the critical frequency will almost certainly depend on amplitude and temperature, the critical exponents would most likely not if the DPT indeed represents a new ''dynamic universality class.'' Finally, we note that the quantities that we have analyzed numerically could all be measured in experiments on hysteresis in a variety of systems and analyzed by methods essentially identical to our analysis of the MC data.

## ACKNOWLEDGMENTS

Thanks are due to M. Acharyya, P. D. Beale, G. Brown, W. Janke, W. Klein, M. Kolesik, G. Korniss, R. A. Ramos, H. L. Richards, H. Tomita, and J. Viñals for helpful discussions. S.W.S. and P.A.R. appreciate hospitality and support from the Colorado Center for Chaos and Complexity during the 1997 Workshop on Nucleation Theory and Phase Transitions. This research was supported in part by the Florida State University Center for Materials Research and Technology, by the FSU Supercomputer Computations Research Institute, which is partially funded by the U.S. Department of Energy through Contract No. DE-FC05-85ER25000, and by the National Science Foundation through Grant Nos. DMR-9315969, DMR-9634873, DMR-9520325, and DMR-9871455. Computing resources at the National Energy Research Scientific Computing Center were made available by the U.S. Department of Energy.

[1] J. A. Ewing, Proc. R. Soc. London **33**, 21 (1881).
[2] E. Warburg, Ann. Phys. Chem. (Neue Folge) **13**, 141 (1881).
[3] J. A. Ewing, Proc. R. Soc. London **34**, 39 (1882).
[4] C. P. Steinmetz, Trans. Am. Inst. Electr. Eng. **9**, 3 (1892).
[5] R. R. Kline, *Steinmetz: Engineer and Socialist* (Johns Hopkins University Press, Baltimore, 1992). We owe most of our knowledge about the early research on hysteresis by Ewing, Warburg, and Steinmetz to this excellent scientific biography.
[6] I. D. Mayergoyz, *Mathematical Models of Hysteresis* (Springer, New York, 1991).
[7] A. Aharoni, *Introduction to the Theory of Ferromagnetism* (Clarendon, Oxford, 1996).
[8] Y. Ishibashi and Y. Takagi, J. Phys. Soc. Jpn. **31**, 506 (1971).
[9] H. Orihara and Y. Ishibashi, J. Phys. Soc. Jpn. **61**, 1919 (1992).
[10] H. M. Duiker and P. D. Beale, Phys. Rev. B **41**, 490 (1990).
[11] P. D. Beale, Integr. Ferroelectr. **4**, 107 (1994).
[12] M. Rao and R. Pandit, Phys. Rev. B **43**, 3373 (1991).
[13] L. Mitoseriu, V. Tura, and A. Stancu, Phys. Lett. A **196**, 272 (1994).
[14] H. Orihara, S. Hashimoto, and Y. Ishibashi, J. Phys. Soc. Jpn. **63**, 1031 (1994).
[15] S. Hashimoto, H. Orihara, and Y. Ishibashi, J. Phys. Soc. Jpn. **63**, 1601 (1994).
[16] A. J. Bard and L. R. Faulkner, *Electrochemical Methods: Fundamentals and Applications* (Wiley, New York, 1980).
[17] P. A. Rikvold, M. Gamboa-Aldego, J. Zhang, M. Han, H. L. Richards, Q. Wang, and A. Wieckowski, Surf. Sci. **335**, 389 (1995).
[18] A. Cheng and M. Chaffrey, J. Phys. Chem. **100**, 5608 (1996).
[19] Z. Peng, K. Krug, and K. Winzer, Phys. Rev. E **57**, R8123 (1998).
[20] G. Burlak and I. Ostrovskiĭ, Tech. Phys. Lett. **23**, 725 (1997).
[21] Y. Martin and H. Wickramasinghe, Appl. Phys. Lett. **50**, 1455 (1987).
[22] T. Chang, J. G. Zhu, and J. Judy, J. Appl. Phys. **73**, 6716 (1993).
[23] M. Lederman, G. Gibson, and S. Schultz, J. Appl. Phys. **73**, 6961 (1993).
[24] M. Lederman, D. Fredkin, R. O'Barr, and S. Schultz, J. Appl. Phys. **75**, 6217 (1994).
[25] M. Lederman, S. Schultz, and M. Ozaki, Phys. Rev. Lett. **73**, 1986 (1994).
[26] H. L. Richards, S. W. Sides, M. A. Novotny, and P. A. Rikvold, J. Magn. Magn. Mater. **150**, 37 (1995).
[27] H. L. Richards, M. A. Novotny, and P. A. Rikvold, Phys. Rev. B **54**, 4113 (1996).
[28] H. L. Richards, M. Kolesik, P.-A. Lindgård, M. A. Novotny, and P. A. Rikvold, Phys. Rev. B **55**, 11 521 (1997).
[29] M. Kolesik, M. A. Novotny, and P. A. Rikvold, Phys. Rev. B **56**, 11 791 (1997).
[30] M. Kolesik, M. A. Novotny, and P. A. Rikvold, in *Microscopic Simulation of Interfacial Phenomena in Solids and Liquids*, edited by S. Phillpot, S. Bristowe, D. Stroud, and J. Smith, MRS Symposia Proceedings No. 492 (Materials Research Society, Pittsburgh, 1998).
[31] P. A. Rikvold, M. A. Novotny, M. Kolesik, and H. L. Richards, in *Dynamical Properties of Unconventional Magnetic Systems*, edited by A. T. Skjeltorp and D. Sherrington (Kluwer, Dordrecht, 1998), p. 307.
[32] Y. He and G.-C. Wang, Phys. Rev. Lett. **70**, 2336 (1993).
[33] J. S. Suen and J. Erskine, Phys. Rev. Lett. **78**, 3567 (1997).
[34] M. Rao, H. Krishnamurthy, and R. Pandit, J. Phys. C **1**, 9061 (1989).
[35] M. Rao, H. Krishnamurthy, and R. Pandit, Phys. Rev. B **42**, 856 (1990).

[36] M. Rao, H. Krishnamurthy, and R. Pandit, J. Appl. Phys. **67**, 5451 (1990).
[37] Q. Jiang, H.-N. Yang, and G.-C. Wang, Phys. Rev. B **52**, 14 911 (1995).
[38] J.-S. Suen, M. H. Lee, G. Teeter, and J. L. Erskine, Phys. Rev. B **59**, 4249 (1999).
[39] A. Visintin, *Differential Models of Hysteresis* (Springer, Berlin, 1994).
[40] M. Brokate and J. Sprekels, *Hysteresis and Phase Transitions* (Springer, New York, 1996).
[41] F. Preisach, Z. Phys. **94**, 277 (1935).
[42] A. H. Nayfeh and B. Balachandran, *Applied Nonlinear Dynamics* (Wiley, New York, 1995).
[43] A. N. Kolmogorov, Bull. Acad. Sci. USSR, Phys. Ser. **1**, 355 (1937).
[44] W. A. Johnson and P. A. Mehl, Trans. Am. Inst. Min. Metall. Eng. **135**, 416 (1939).
[45] M. Avrami, J. Chem. Phys. **7**, 1103 (1939); **8**, 212 (1940); **9**, 177 (1941).
[46] This elementary relation was regrettably misprinted in Ref. [50] .
[47] H. Tomita and S. Miyashita, Phys. Rev. B **46**, 8886 (1992).
[48] P. A. Rikvold, H. Tomita, S. Miyashita, and S. W. Sides, Phys. Rev. E **49**, 5080 (1994).
[49] P. A. Rikvold and B. M. Gorman, in *Annual Reviews of Computational Physics I*, edited by D. Stauffer (World Scientific, Singapore, 1994), p. 149.
[50] S. W. Sides, P. A. Rikvold, and M. A. Novotny, Phys. Rev. E **57**, 6512 (1998).
[51] S. W. Sides, R. A. Ramos, P. A. Rikvold, and M. A. Novotny, J. Appl. Phys. **79**, 6482 (1996); **81**, 5597 (1997).
[52] S. W. Sides, P. A. Rikvold, and M. A. Novotny, J. Appl. Phys. **83**, 6494 (1998).
[53] A recent review is given in B. Chakrabarti and M. Acharyya, e-print cond-mat/9811086.
[54] P. Jung, G. Gray, and R. Roy, Phys. Rev. Lett. **65**, 1873 (1990).
[55] T. Tomé and M. J. de Oliveira, Phys. Rev. A **41**, 4251 (1990).
[56] C. Luse and A. Zangwill, Phys. Rev. E **50**, 224 (1994).
[57] M. Acharyya and B. K. Chakrabarti, in *Annual Reviews of Computational Physics I*, edited by D. Stauffer (World Scientific, Singapore, 1994), p. 107.
[58] M. Acharyya and B. K. Chakrabarti, Physica A **192**, 471 (1992).
[59] M. Acharyya, B. K. Chakrabarti, and A. K. Sen, Physica A **186**, 231 (1992).
[60] M. Acharyya and B. K. Chakrabarti, J. Magn. Magn. Mater. **136**, L29 (1994).
[61] M. Acharyya, B. K. Chakrabarti, and R. Stinchcombe, J. Phys. A **27**, 1533 (1994).
[62] W. Lo and R. A. Pelcovits, Phys. Rev. A **42**, 7471 (1990).
[63] Z. Fan, Z. Jinxiu, and L. Xiao, Phys. Rev. E **52**, 1399 (1995).
[64] M. Acharyya, Phys. Rev. E **56**, 1234 (1997).
[65] M. Acharyya, Physica A **235**, 469 (1997).
[66] M. Acharyya and B. K. Chakrabarti, Phys. Rev. B **52**, 6550 (1995).
[67] D. Dhar and P. B. Thomas, J. Phys. A **25**, 4967 (1992).
[68] P. B. Thomas and D. Dhar, J. Phys. A **26**, 3973 (1993).
[69] S. W. Sides, P. A. Rikvold, and M. A. Novotny, Phys. Rev. Lett. **81**, 834 (1998).
[70] K. A. Dahmen and J. P. Sethna, Phys. Rev. Lett. **71**, 3222 (1993).
[71] R. Glauber, J. Math. Phys. **4**, 294 (1963).
[72] K. Binder and D. Heermann, *Monte Carlo Simulation in Statistical Physics*, 3rd ed. (Springer, Berlin, 1997).
[73] P. A. Martin, J. Stat. Phys. **16**, 149 (1977).
[74] J. S. Langer, Ann. Phys. (N.Y.) **41**, 108 (1967); **54**, 258 (1969).
[75] N. J. Günther, D. A. Nicole, and D. J. Wallace, J. Phys. A **13**, 1755 (1980).
[76] C. C. A. Günther, P. A. Rikvold, and M. A. Novotny, Phys. Rev. Lett. **71**, 3898 (1993).
[77] C. C. A. Günther, P. A. Rikvold, and M. A. Novotny, Physica A **212**, 194 (1994).
[78] See, e.g., Y. C. Chiew and E. D. Glandt, J. Colloid Interface Sci. **99**, 86 (1984); P. A. Rikvold and G. Stell, *ibid.* **108**, 158 (1985), and references cited therein.
[79] R. A. Ramos, P. A. Rikvold, and M. A. Novotny, e-print cond-mat/9811079.
[80] J. Lee, M. A. Novotny, and P. A. Rikvold, Phys. Rev. E **52**, 356 (1995).
[81] V. Shneidman, P. Jung, and P. Hänggi, Europhys. Lett. **26**, 571 (1994); Phys. Rev. Lett. **72**, 2682 (1994).
[82] M. Acharyya, Phys. Rev. E **58**, 179 (1998).
[83] J. Gunton and M. Droz, *Introduction to the Theory of Metastable and Unstable States* (Springer, Berlin, 1983).
[84] I. Lifshitz, Zh. Éksp. Teor. Fiz. **42**, 1354 (1962) [Sov. Phys. JETP **15**, 939 (1962)].
[85] S. Allen and J. Cahn, Acta Metall. **27**, 1085 (1979).
[86] V. A. Shneidman and M. C. Weinberg, J. Non-Cryst. Solids **160**, 89 (1993); Ceram. Trans. **30**, 225 (1993).
[87] V. A. Shneidman, K. A. Jackson, and K. M. Beatty, Phys. Rev. B **59**, 3579 (1999).
[88] S. Sengupta, Y. Marathe, and S. Puri, Phys. Rev. B **45**, 7828 (1992).
[89] *Handbook of Mathematical Functions*, edited by M. Abramowitz and I. A. Stegun, Natl. Bur. Stand. U.S. (U.S. GPO, Washington, DC, 1970), p. 260.
[90] L. Gammaitoni, P. Hänggi, P. Jung, and F. Marchesoni, Rev. Mod. Phys. **70**, 223 (1998).
[91] K. Binder, in *Finite Size Scaling and Numerical Simulation of Statistical Systems*, edited by V. Privman (World Scientific, Singapore, 1990).
[92] K. Huang, *Statistical Mechanics* (Wiley, New York, 1987).
[93] K. Eichhorn and K. Binder, Z. Phys. B **99**, 413 (1996).
[94] G. Kamieniarz and H. Blöte, J. Phys. A **26**, 201 (1993).
[95] K. K. Mon, Phys. Rev. B **55**, 38 (1997).
[96] E. Luijten, K. Binder, and H. W. J. Blöte, Eur. Phys. J. B (to be published). It is instructive to keep in mind that finite-size scaling results based on a limited range of system sizes can be misleading, even for such an extensively studied system as the five-dimensional Ising ferromagnet in equilibrium.
[97] E. Brézin and J. Zinn-Justin, Nucl. Phys. B **257 [FS14]**, 867 (1985).
[98] G. Korniss (private communication).
[99] M. Paniconi and Y. Oono, Phys. Rev. E **55**, 176 (1997).